AGV-Assisted Adaptive Cooperative Transmission for State Estimation in Industrial IoT Systems

Ling Lyu, *Member, IEEE*, Zexin Qiao, Yanpeng Dai, *Member, IEEE*, Nan Cheng, *Senior Member, IEEE*, Cailian Chen, *Member, IEEE*, Xinping Guan, *Fellow, IEEE*, and Xuemin Shen, *Fellow, IEEE*

***Abstract*—The wide application of Internet of Things (IoT) technology in industrial automation promotes the emergence of industrial IoT systems, in which state estimation plays a crucial role in conjecturing system states with sensory data delivered over wireless channels. In this paper, we propose an automated guided vehicle (AGV)-assisted adaptive cooperative transmission scheme to minimize the mean square error of state estimation at a low energy cost. Specifically, a novel performance index, estimation gain, is introduced to evaluate the benefit of scheduling one sensor for estimation error reduction. Then, sensor scheduling and data transmission are jointly optimized to minimize the time-accumulated estimation error, which is challenging to directly solve due to the unclear impact of imperfect transmission on estimation performance. To this end, an estimation gain-based algorithm is designed to determine the scheduled sensors. Besides, an iterative algorithm is designed to solve the adaptive cooperative transmission problem. Simulation results show that the proposed scheme outperforms benchmark schemes in reducing estimation error and energy consumption.**

***Index Terms*—AGV, cooperative transmission, industrial IoT systems, sensor scheduling, state estimation.**

I. Introduction

INTERNET of Things (IoT) technology have been widely used in actual industrial systems such as equipment predictive maintenance, production efficiency control and intelligent logistics, promoting the emergence of industrial IoT systems [1], [1], [2], [3], [4], [5], [6]. In industrial IoT systems, sensors are widely deployed to collect sensory data, which is then used by the remote controller to perform state estimation to conjecture the operating status of industrial process [7], [8], [9]. Therefore, the performance of state estimation heavily relies on the transmission performance, since to information exchange through the network [10], [11], [12]. However, the unreliability of wireless channels and the complex and dynamic industrial transmission environment result in poor transmission performance, making it challenge to achieve high-accuracy state estimation for industrial IoT systems [13].

Recently, there has been considerable research interest in studying state estimation algorithms to mitigate the impact of transmission unreliability on the state estimation accuracy. Ding et al. [14] investigated the data fusion estimation problem for multi-sensor network systems, and proposed a matrix fusion estimation algorithm to improve the estimation performance by prediction compensation strategy. Yang et al. [15] designed a state estimation algorithm based on an observation network to mitigate the impact of partial sensor failures on the accuracy of state estimation. Liu et al. [16] proposed an estimation-cycle-based algorithm to mitigate the impact of time-varying packet drop probability and Markov fading channel. Dai et al. [17] analyzed the impact of random delay on the accuracy of state estimation, and developed a fusion estimation method based on a hierarchical network architecture to reduce the error of state estimation. Feng et al. [18] discussed the state estimation of systems with white Gaussian noise and power disturbance on unreliable links, and proposed a cascaded estimation algorithm to improve the robustness of estimation performance. The above work mainly focuses on designing state estimation strategies to passively mitigate the impact of adverse transmission environment on the performance of state estimation. Due to the estimation performance heavily depends on the transmission performance, another way of improving the estimation performance is to proactively enhance the transmission efficiency and reliability by designing on-demand transmission scheme for state estimation [19].

Cooperative transmission is regarded as an important technology to improve the transmission reliability with utilization of spatial diversity gain [20], [21], [22]. Mao et al. [23] proposed a cooperative transmission protocol to guarantee the transmission fairness of users in the group to maximize the

Received 9 April 2024; revised 18 August 2024 and 19 September 2024; accepted 25 September 2024. Date of publication 1 October 2024; date of current version 14 February 2025. This work was supported in part by the National Natural Science Foundation of China under Grant 62002042, Grant 62101089, Grant 62071356, Grant 92167205, and Grant 61933009, in part by the China Postdoctoral Science Foundation under Grant 2021M700655, in part by the Fundamental Research Funds for the Central Universities under Grant JB210113, in part by the Doctoral Research Startup Funds of Liaoning Province under Grant 2023-BS-068, and in part by the Fundamental Research Funds for Central Universities under Grant 3132024245. The review of this article was coordinated by Dr. Lan Zhang. *(Corresponding author: Yanpeng Dai.)*

Ling Lyu is with the School of Information Science and Technology, Dalian Maritime University, Dalian 116026, China, and also with the Key Laboratory of System Control and Information Processing, Ministry of Education of China, Shanghai 200240, China (e-mail: linglyu@dlmu.edu.cn).

Zexin Qiao and Yanpeng Dai are with the School of Information Science and Technology, Dalian Maritime University, Dalian 116026, China (e-mail: zexinqiao@dlmu.edu.cn; yanpengdai@dlmu.edu.cn).

Nan Cheng is with the Key State Lab. of ISN and School of Telecommunications Engineering, Xidian University, Xi'an 710071, China (e-mail: dr.nan.cheng@ieee.org).

Cailian Chen and Xinping Guan are with the Department of Automation, Shanghai Jiao Tong University, Shanghai 200240, China, and also with the Key Laboratory of System Control and Information Processing, Ministry of Education of China, Shanghai 200240, China (e-mail: cailianchen@sjtu.edu.cn; xpguan@sjtu.edu.cn).

Xuemin Shen is with the Department of Electrical and Computer Engineering, University of Waterloo, Waterloo, ON N2L 3G1, Canada (e-mail: sshen@uwaterloo.ca).

Digital Object Identifier 10.1109/TVT.2024.3472030

0018-9545 © 2024 IEEE. Personal use is permitted, but republication/redistribution requires IEEE permission.
See https://www.ieee.org/publications/rights/index.html for more information.

Authorized licensed use limited to: University of Waterloo. Downloaded on March 04,2025 at 21:56:16 UTC from IEEE Xplore. Restrictions apply.

minimum throughput, and showed that cooperative transmission can achieve higher throughput under the same transmission conditions and be more energy-efficient in harsh transmission environments. Xu et al. [24] proposed a buffer-assisted cooperative transmission system that adaptively selects transmission modes based on buffer status to reduce packet delay and outage probability. Tuan et al. [25] analyzed the performance of various transmission schemes in industrial wireless sensor network, and the results showed that compared with non-cooperative transmission schemes such as amplify-and-forward and decode-and-forward, incremental cooperative transmission schemes can better balance the relationship between energy consumption and throughput. Kim et al. [26] proposed a cooperative multi-hop relay transmission scheme to reduce the total energy consumption of the system. Chae et al. [27] investigated cooperative relaying transmission in multi-user multiple-input multiple-output wireless networks, and proposed a new cooperative relaying transmission scheme to improve the multiplexing gain of multiple antennas. Inspired by the advantages of cooperative transmission in improving network transmission performance, it is reasonable to apply cooperative transmission to industrial IoT systems to improve the accuracy of state estimation. However, it is not suitable to directly apply the existing cooperative transmission scheme to the considered state estimation in industrial network systems, since different sensors have distinct sensing abilities and observation noises. Moreover, even though the transmission performances between different sensors and the remote estimator are the same, the contribution to reducing estimation error is different.

Although cooperative transmission has the advantage to improve the transmission performance, placing additional specialized devices only for the purpose of forwarding information to the remote estimator is not cost-effective. With the increasing application of automated guided vehicles (AGVs) in the industrial field [28], [29], [30], AGVs are applied in industrial plant for delivering heavy and/or bulky pieces between manufacturing stations due to the high degree of autonomy and flexibility. However, when the AGV goes across the plant, AGV may be regarded as the obstacle and then makes sensors be in the occlusion areas and suffer the severe shadow fading. In this case, the line-of-sight transmission link between sensors and the remote estimator will be broken, leading to the transmission rate reduction. As a solution, wireless transceivers are equipped to AGV, and then AGV is employed to construct the cooperative transmission architecture by regarding it as a relay. In this way, AGV could help forward the received sensory data from sensors to remoter estimator, making it possible to improve the end-to-end data transmission performance.

In this paper, we design an AGV-assisted adaptive cooperative transmission scheme in industrial IoT systems. On one hand, we consider two transmission modes (i.e., cooperative transmission mode and direct transmission mode), and choose the appropriate transmission mode based on the channel gain between sensors and remote estimator. Only when the line-of-sight transmission link between sensors and remote estimator is heavily obstructed by AGV, the AGV-assisted cooperative transmission mode is activated. On the other hand, as sensors are generally powered with batteries, sensors with insufficient energy will enter a low-energy consumption mode. Therefore, only a part of sensors will engage in state estimation, with each sensor autonomously determining its participation. The contributions of this paper are summarized as follows.

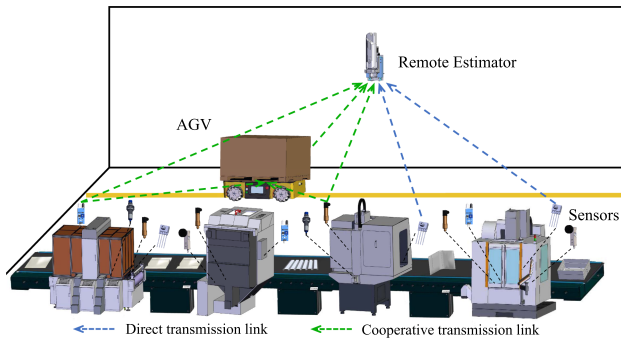

Fig. 1. AGV-assisted cooperative transmission industry IoT system.

- A novel performance index, estimation gain, is proposed to evaluate the benefit of scheduling one sensor for estimation error reduction, which makes it possible to design an appropriate sensor scheduling algorithm for minimizing estimation error.
- We design an adaptive cooperative transmission scheme based on the presented rate utility index, which minimizes the time-accumulated mean square error guarantees the maximum amount of delivered sensory data by jointly optimizing the sensor scheduling and data transmission.
- An estimation gain-based algorithm is designed to determine the scheduled sensors, which could effectively deal with the unclear impact of the imperfect transmission on estimation performance. Moreover, a Lagrangian-penalty method based iterative algorithm is proposed to address the power coupling problem between sensors and AGV in cooperative transmission mode.

The remainder of this paper is organized as follows. The system model and problem formulation is presented in Section II. In Section III, adaptive cooperative transmission scheme is studied to minimize the mean square estimation error. Simulation results and main conclusions are shown in Sections IV and V, respectively.

II. System Model and Problem Formulation

In industrial IoT systems, multiple sensors are deployed and cooperatively sense system situations to complete the monitoring task. Sensors could monitor the operational status of equipment and transmit the sensory data to the remote estimator (RE). Based on the received sensory data, the RE performs the state estimation to conjecture the operational status of industrial process. In the considered scenario, AGV plays the role of a relay node, thus it could forward the received signal from sensors to RE, as shown in Fig. 1.

A. Network Model

The considered AGV-assisted industrial IoT system is composed of one RE, one AGV and a set of sensors $\mathcal{N} =$

Authorized licensed use limited to: University of Waterloo. Downloaded on March 04,2025 at 21:56:16 UTC from IEEE Xplore. Restrictions apply.

$\{1, 2, \ldots, N\}$. In the considered scenario, AGV is already existed in the plant, which is used to carry cargoes. The three-dimensional Euclidean coordinate system is adopted to describe the locations of sensors and RE. The location of n-th sensor and RE is respectively denoted by $z_n = [x_n, y_n, 0]$ and $z_{\mathrm{R}} = [x_{\mathrm{R}}, y_{\mathrm{R}}, H_{\mathrm{R}}]$, where H_{R} is the altitude of RE. Path planning refers to finding collision-free handling paths that meet the requirements of AGV operation according to the ruls set in advance (with the least time or the shortest distance) when AGV carries out cargo handling tasks. In this case, AGV's trajectory is determined by the logistics management unit to achieve the high-efficient material transportation. Assume that AGV carries the cargo and passes through the target area along a fixed trajectory at a constant speed v in duration T_{A}. The duration T_{A} includes K estimation steps that is denoted by $\mathcal{K} = \{1, 2, \ldots, K\}$. The duration of one estimation step τ is sufficiently small so that the AGV could be regarded as static. The location of AGV at the k-th estimation step is $z_{\mathrm{A}}(k) = [x_{\mathrm{A}}(k), y_{\mathrm{A}}(k), H_{\mathrm{A}}]$, where H_{A} is the antenna height of AGV.

The available spectrum resource consists of a set of subcarriers $\mathcal{M} = \{1, 2, \ldots, M\}$. The bandwidth of each subcarrier is B. Let binary variable $\theta_{n,m}(k)$ denote the association relationship between n-th sensor and m-th subcarrier. $\theta_{n,m}(k) = 1$ denotes that the m-th subcarrier is allocated to the n-th sensor at the k-th estimation step. Otherwise, $\theta_{n,m}(k) = 0$. To avoid severe co-channel interference, one subcarrier could be allocated to at most one sensor at one estimation step, i.e.,

$$\sum_{n\in\mathcal{N}} \theta_{n,m}(k) \le 1,\ m \in \mathcal{M},\ k \in \mathcal{K}. \tag{1}$$

As mentioned above, the performance of state estimation is affected by the amount of sensory data successfully received by the RE. The estimation performance sharply decline if the data amount is below a threshold [31]. In order to ensure that the estimation accuracy is within a controllable range, it yields that

$$N_{\min} \le \sum_{n\in\mathcal{N}} \xi_n(k) \le M,\ k \in \mathcal{K}, \tag{2}$$

where $\xi_n(k)$ is the sensor-scheduling indicator. $\xi_n(k) = 1$ denotes that the n-th sensor is scheduled to transmit data at the k-th estimation step. Otherwise, $\xi_n(k) = 0$. $N_{\min}$ is the minimum number of scheduled sensors in each estimation step. For scheduled sensors, two transmission modes are considered in this work:

- *Cooperative transmission mode:* AGV works in the half-duplex mode. Each estimation step is partitioned into two stages, as shown in Fig. 2. In the first transmission stage, sensor broadcasts sensory data to both AGV and RE. Then, AGV amplifies the received data and forwards it to RE in the second transmission stage.
- *Direct transmission mode:* Sensors transmit the sensory data to RE directly.

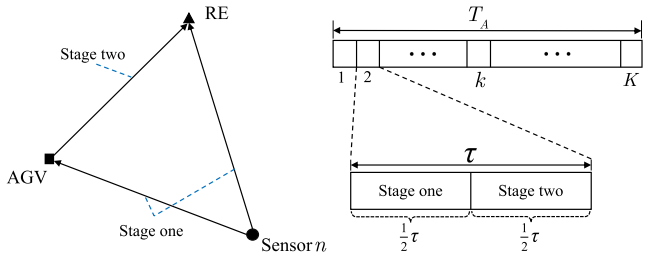

Fig. 2. Two-stage data transmission diagram and estimation step division in cooperative mode.

Let binary variable $\delta_n(k)$ denote the transmission mode of sensors in k-th estimation step,

$$\delta_n(k) = \begin{cases} 1, & n\text{-th sensor in the cooperative transmission mode,} \\ 0, & n\text{-th sensor in the direct transmission mode.} \end{cases} \tag{3}$$

B. Transmission Model

In this subsection, we present data transmission models for the direct transmission and cooperative transmission modes.

1) Direct Transmission Mode: At the k-th estimation step, the channel power gain between the n-th sensor and RE on the m-th subcarrier is given by

$$h^{\mathrm{SR}}_{n,m}(k) = g_m(k) l^{\mathrm{SR}}_{I,n},\ n \in \mathcal{N}, k \in \mathcal{K}, \tag{4}$$

where $g_m(k)$ denotes the Rayleigh small scale fading satisfying $g_m(k) \sim \mathcal{CN}(0, 1)$ and $l^{\mathrm{SR}}_{I,n}$ denotes the pathloss. Multi-slope bounded pathloss model (MBPM) [32] is applied to characterize the signal attenuation with long and short propagation distance. In particular, MBPM is given by

$$l^{\mathrm{SR}}_{I,n} = \mu_i \left(1 + (d^{\mathrm{SR}}_n)^{\beta_i}\right)^{-1},\ D_i \le d^{\mathrm{SR}}_n \le D_{i+1}, \tag{5}$$

where d^{SR}_n denotes the distance between the n-th sensor and RE. D_i denotes corner distance with $0 = D_0 < D_1 < \cdots < D_I = \infty$. Note that the pathloss exponents β_i are different within different $[D_i, D_{i+1})$. Furthermore, let $\mu_0 = 1$ and $\mu_i = \prod_{j=1}^{i} \frac{1+D_j^{\beta_j}}{1+D_j^{\beta_{j-1}}} (i > 0)$. The SNR of the direct link between the n-th sensor and RE can be expressed as

$$\Gamma^{\mathrm{D}}_{n,m}(k) = p^{\mathrm{S}}_{n,m}(k) \gamma^{\mathrm{SR}}_{n,m}(k), \tag{6}$$

where $p^{\mathrm{S}}_{n,m}(k)$ is the transmit power of the n-th sensor on the m-th subcarrier. $\gamma^{\mathrm{SR}}_{n,m}(k) = h^{\mathrm{SR}}_{n,m}(k)/\sigma^2$ is the SNR of unit power between the n-th sensor and RE. σ^2 is the noise power. The direct transmission rate of the n-th sensor can be expressed as

$$R^{\mathrm{D}}_n(k) = \sum_{m\in\mathcal{M}} \theta_{n,m}(k) B \log_2\left(1 + \Gamma^{\mathrm{D}}_{n,m}(k)\right). \tag{7}$$

The direct transmission delay of the n-th sensor at the k-th estimation step is

$$t^{\mathrm{D}}_n(k) = \frac{q_n(k)}{R^{\mathrm{D}}_n(k)}, \tag{8}$$

Authorized licensed use limited to: University of Waterloo. Downloaded on March 04,2025 at 21:56:16 UTC from IEEE Xplore. Restrictions apply.

where $q_n(k)$ is the length of data packet generated by the n-th sensor at the k-th estimation step.

2) Cooperative Transmission Mode: The sensor broadcasts sensory data to AGV and RE in the first transmission stage. In the second transmission stage, AGV relays the received data to RE. Then, RE combines the signals received from sensor and AGV with the maximal ratio combining technique. Thus, the SNR of cooperative transmission between the n-th sensor and RE is expressed as

$$\Gamma^{\mathrm{C}}_{n,m}(k) = \Gamma^{\mathrm{D}}_{n,m}(k) + \Gamma^{\mathrm{R}}_{n,m}(k), \tag{9}$$

where $\Gamma^{\mathrm{R}}_{n,m}(k)$ is the SNR of the two-hop relay link between the n-th sensor and RE through the AGV. $\Gamma^{\mathrm{R}}_{n,m}(k)$ is shown as

$$\begin{aligned}\Gamma^{\mathrm{R}}_{n,m}(k) &= \frac{p^{\mathrm{S}}_{n,m}(k)\gamma^{\mathrm{SA}}_{n,m}(k)p^{\mathrm{A}}_{n,m}(k)\gamma^{\mathrm{AR}}_{n,m}(k)}{1+p^{\mathrm{S}}_{n,m}(k)\gamma^{\mathrm{SA}}_{n,m}(k)+p^{\mathrm{A}}_{n,m}(k)\gamma^{\mathrm{AR}}_{n,m}(k)} \\ &\simeq \frac{p^{\mathrm{S}}_{n,m}(k)\gamma^{\mathrm{SA}}_{n,m}(k)p^{\mathrm{A}}_{n,m}(k)\gamma^{\mathrm{AR}}_{n,m}(k)}{p^{\mathrm{S}}_{n,m}(k)\gamma^{\mathrm{SA}}_{n,m}(k)+p^{\mathrm{A}}_{n,m}(k)\gamma^{\mathrm{AR}}_{n,m}(k)},\end{aligned} \tag{10}$$

where $\gamma^{\mathrm{SA}}_{n,m}(k) = h^{\mathrm{SA}}_{n,m}(k)/\sigma^2$ is the SNR of unit power between the n-th sensor and AGV. $\gamma^{\mathrm{AR}}_{n,m}(k) = h^{\mathrm{AR}}_{n,m}(k)/\sigma^2$ is the SNR of unit power between AGV and RE. $p^{\mathrm{A}}_{n,m}(k)$ is the transmit power of AGV for forwarding the sensory data of the n-th sensor on the m-th subcarrier. The approximation of $\Gamma^{\mathrm{R}}_{n,m}(k)$ in (10) is tight at higher SNR values [33] and it is also valid at low SNR values [34]. According to [35], the cooperative transmission rate of the n-th sensor can be expressed as

$$R^{\mathrm{C}}_n(k) = \frac{1}{2}\sum_{m\in\mathcal{M}} \theta_{n,m}(k) B \log_2\left(1+\Gamma^{\mathrm{C}}_{n,m}(k)\right). \tag{11}$$

The cooperative transmission delay of the n-th sensor at the k-th estimation step is given by

$$t^{\mathrm{C}}_n(k) = \frac{q_n(k)}{R^{\mathrm{C}}_n(k)}. \tag{12}$$

Then, the overall transmission delay experienced by the sensory data generated by the n-th sensor is given by

$$t_n(k) = \left(1-\delta_n(k)\right) t^{\mathrm{D}}_n(k) + \delta_n(k) t^{\mathrm{C}}_n(k). \tag{13}$$

As sensors are generally powered with batteries, energy consumption is a key performance index. In order to save energy and prolong the working life, only a part of sensors will participate in state estimation. Non-participating sensors will be in the sleeping state. The energy consumption in the sleeping state is $E^{\mathrm{D}} = E^{\mathrm{D}}_0 \tau$, where the E^{D}_0 is the energy consumption of the sensor per unit time. When sensors are scheduled to transmit data, the main energy consumption is caused by data transmission. The transmission energy consumption of the n-th sensor at the k-th estimation step is given by

$$E^{\mathrm{T}}_n(k) = \sum_{m\in\mathcal{M}} \theta_{n,m}(k) p^{\mathrm{S}}_{n,m}(k) t_n(k). \tag{14}$$

Therefore, the total energy consumption of the n-th sensor at the k-th estimation step is

$$E^{\mathrm{C}}_n(k) = \xi_n(k) E^{\mathrm{T}}_n(k) + \left(1-\xi_n(k)\right) E^{\mathrm{D}}. \tag{15}$$

The residual energy of the n-th sensor at the end of the k-th estimation step is

$$E^{\mathrm{R}}_n(k) = E^{\mathrm{R}}_n(k-1) - E^{\mathrm{C}}_n(k), \tag{16}$$

where $E^{\mathrm{R}}_n(k-1)$ is the residual energy for the n-th sensor at the end of the $(k-1)$-th estimation step.

C. State Estimation Model

The considered industrial process is sensed by N sensors. According to Refs. [36], [37], [38], [39], [40], [41], the dynamic control system is modeled as

$$x(k+1) = Ax(k) + w(k), \tag{17}$$

where $x(k) \in \mathbb{R}^{r_x}$ is the system state at the k-th control step, $A \in \mathbb{R}^{r_x \times r_x}$ is state transition matrix, and $w(k) \in \mathbb{R}^{r_x}$ is process noise. Moreover, the observation-based state estimation is expressed as

$$y_n(k) = C_n x(k) + v_n(k),\ n \in \mathcal{N}, \tag{18}$$

where $y_n(k) \in \mathbb{R}^{r_y}$ is the measurement of the n-th sensor at the k-th control step, $C_n \in \mathbb{R}^{r_y \times r_x}$ is the measurement matrix of the n-th sensor, and $v_n(k) \in \mathbb{R}^{r_y}$ is the measurement noise. The initial state $x(0)$ is a Gaussian random vector with the mean $\bar{x}_0$ and covariance matrix W_0. We assume the process noise $w(k) \in \mathbb{R}^{r_x}$ and measurement noise $v_n(k) \in \mathbb{R}^{r_y}$ are independent and are identically distributed zero-mean Gaussian processes with corresponding covariance matrices Q_w and Q_v, respectively [16].

Then, the observation-based state estimation could be expressed in an aggregated form, shown as $y(k) = C_R x(k) + v(k)$, where $y(k) = [y_1^T(k), \ldots, y_N^T(k)]^T$, $C_R = [C_1^T, \ldots, C_N^T]^T$, and $v(k) = [v_1^T(k), \ldots, v_N^T(k)]^T$. Let $\Lambda(k)$=diag$\{\xi_1(k)\zeta_1(k)\mathbf{I}_1(k), \ldots, \xi_N(k)\zeta_N(k)\mathbf{I}_N(k)\}$, the aggregated observation matrix is

$$\tilde{C}_R(k) = \Lambda(k) C_R. \tag{19}$$

Due to the rugged industrial environment, some raw observation information may not be received successfully by RE. Let binary variable $\zeta_n(k)$ denote the receive status of data packet at RE which is defined as

$$\zeta_n(k) = \begin{cases} 1, & \text{if } t_n(k) \le \tau, \\ 0, & \text{otherwise.} \end{cases} \tag{20}$$

Moreover, since some scheduled sensors may not participate the state estimation due to limited energy, the available observation at RE at the k-th estimation step is

$$\tilde{y}(k) \triangleq \left[\xi_1(k)\zeta_1(k)y_1^T(k), \ldots, \xi_N(k)\zeta_N(k)y_N^T(k)\right]^T. \tag{21}$$

According to Refs. [14], the observation based state estimation is expressed as $\hat{x}(k|k) = \hat{x}(k|k-1) + F(\tilde{y}(k) - \hat{y}(k|k-1))$, where F is the correction matrix of observation. The one-step prediction of observation is $\hat{y}(k|k-1) = \tilde{C}_R(k)\hat{x}(k|k-$

Authorized licensed use limited to: University of Waterloo. Downloaded on March 04,2025 at 21:56:16 UTC from IEEE Xplore. Restrictions apply.

1), where $\hat{x}(k|k-1) = A\hat{x}(k-1|k-1)$. Then, the observation based state estimation can be rewritten as

$$\hat{x}(k|k)=A\hat{x}(k-1|k-1)+F\left(\tilde{y}(k)-\tilde{C}_R(k)A\hat{x}(k-1|k-1)\right). \tag{22}$$

The estimation error is defined as the gap between the true state $x(k)$ and the estimated value $\hat{x}(k|k)$ at remote estimator, i.e., $e(k) = x(k) - \hat{x}(k|k)$. As $x(k) = Ax(k-1) + w(k-1)$, we can obtain that $e(k) = [Ax(k-1) + w(k-1)] - \hat{x}(k|k)$. Then, $e(k) = Ae(k-1) + w(k-1) - F[\tilde{y}(k) - \tilde{C}_R(k)A\hat{x}(k-1|k-1)]$. As $\tilde{y}(k) = \Lambda(k)y(k)$, we can obtain that $\tilde{y}(k) - \tilde{C}_R(k)A\hat{x}(k-1|k-1) = \tilde{C}_R(k)(Ae(k-1) + w(k-1)) + \tilde{v}(k)$. Then,

$$\begin{aligned} e(k) &= x(k) - \hat{x}(k|k) \\ &= \left(A-AF\tilde{C}_R(k)\right)e(k-1)-\tilde{v}(k)+\left(I-F\tilde{C}_R(k)\right)w(k-1), \end{aligned} \tag{23}$$

where $\tilde{v}(k) = [\xi_1(k)\zeta_1(k)v_1^T(k), \ldots, \xi_N(k)\zeta_N(k)v_N^T(k)]^T$.

In summary, the transmission models include sensor scheduling, transmission mode selection, and channel allocation with power control. To be specific, different sensors have distinct sensing abilities and observation noises, thus scheduling different sensors will have distinct contributions to reducing the estimation error. In this way, sensor scheduling can affect the state estimation performance. Besides, the achievable transmission rates of sensory data are different in the cooperative transmission mode and the direct transmission mode. Thus, transmission mode selection has the ability to enlarge the transmission rate by adaptively adjusting the transmission mode based on the status of wireless channels. Moreover, channel allocation with power control also affects the transmission rate of sensory data, which in turn determines the probability of successfully delivering one packet within the deadline. Therefore, sensor scheduling, transmission mode selection, and channel allocation with power control have a tight impact on the performance of state estimation. In this paper, the trace of mean square estimation error $\mathrm{Tr}\left(\mathbb{E}\{\|e(k)\|_2^2\}\right)$ is employed to evaluate the estimation performance.

D. Problem Formulation

We aims to minimize the mean square error of state estimation by jointly optimizing the sensor scheduling, transmission mode selection, subcarrier allocation and transmit power. The estimation error minimization problem is formulated as

$$\mathcal{P}_0: \min_{\boldsymbol{\xi},\boldsymbol{\delta},\boldsymbol{\theta},\boldsymbol{p}^{\mathrm{S}},\boldsymbol{p}^{\mathrm{A}}} \frac{1}{K}\sum_{k\in\mathcal{K}} \mathrm{Tr}\left(\mathbb{E}\left\{\|e(k)\|_2^2\right\}\right) \tag{24}$$

$$\text{s.t. } N_{\min} \le \sum_{n\in\mathcal{N}} \xi_n(k) \le M, \tag{24a}$$

$$\sum_{n\in\mathcal{N}} \theta_{n,m}(k) \le 1, \ \forall m \in \mathcal{M}, \tag{24b}$$

$$\sum_{m\in\mathcal{M}} \xi_n(k)\theta_{n,m}(k)p_{n,m}^{\mathrm{S}}(k) \le p_{\max}^{\mathrm{S}}, \forall n \in \mathcal{N}, \tag{24c}$$

$$\sum_{n\in\mathcal{N}}\sum_{m\in\mathcal{M}} \xi_n(k)\delta_n(k)\theta_{n,m}p_{n,m}^{\mathrm{A}}(k) \le p_{\max}^{\mathrm{A}}, \tag{24d}$$

$$\theta_{n,m}(k) \in \{0,1\}, \forall n \in \mathcal{N}, \forall m \in \mathcal{M}, \tag{24e}$$

$$\delta_n(k) \in \{0,1\}, \ \forall n \in \mathcal{N}, \tag{24f}$$

$$\xi_n(k) \in \{0,1\}, \ \forall n \in \mathcal{N}, \tag{24g}$$

$$\xi_n(k) = 0, n \in \left\{j | E_j^{\mathrm{R}}(k) < E_{\min}^{\mathrm{R}}, \forall j \in \mathcal{N}\right\}, \tag{24h}$$

where $p_{\max}^{\mathrm{S}}$ and $p_{\max}^{\mathrm{A}}$ are the maximum transmit power of sensor and AGV, respectively. Constraint (24a) limits the number of sensors scheduled at each estimation step. Constraint (24b) restricts that one subcarrier could be assigned to at most one sensor. Constraints (24e), (24f) and (24g) describe the feasible regions of indicator variables. Constraint (24h) means that sensors without enough residual energy cannot be scheduled.

III. Adaptive Cooperative Transmission

Note that $\mathcal{P}_0$ is a mixed-integer nonlinear programming (MINLP) problem, since it includes a nonlinear objective function and mixed-integer variables (binary variables ξ, δ and θ, continuous variables $\boldsymbol{p}^{\mathbf{S}}$ and $\boldsymbol{p}^{\mathbf{A}}$). As the objective function of $\mathcal{P}_0$ includes the time-accumulated term of estimation error, it is challenging to solve this problem efficiently. As a solution, the original problem is decomposed into K problems, and each problem aims to minimize the instantaneous estimation error $\mathrm{Tr}\left(\mathbb{E}\{\|e(k)\|_2^2\}\right)$. As the instantaneous estimation error cannot be expressed explicitly with decision variables, it is still intractable to solve it. With insight into the instantaneous estimation error, we find that it is directly affected by the sensor scheduling and the transmission status of sensory data. In addition, there is a sequential relationship between sensor scheduling and transmission status of sensory data. In other words, only the scheduled sensors concern about the transmission status of sensory data. Therefore, the problem at each estimation step is further decomposed into two sequential subproblems. One is the sensor scheduling subproblem, and the other is the sensory data transmission subproblem. When the transmission status of sensory data is given (i.e., $\zeta_n(k) = 1, \forall n \in \mathcal{N}$), the sensor scheduling subproblem at the k-th estimation step is expressed as

$$\begin{aligned} \mathcal{SP}_1: \min_{\boldsymbol{\xi}} \ & \mathrm{Tr}\left(\mathbb{E}\left\{\|e(k)\|_2^2\right\}\right) \\ \text{s.t. } & \text{(24a), (24g), (24h).} \end{aligned} \tag{25}$$

After sensor scheduling is obtained, transmission mode selection, subcarrier allocation, and power control are jointly optimized to further enlarge the amount of sensory data successfully received by RE. The sensory data transmission subproblem at the k-th estimation step is expressed as

$$\mathcal{SP}_2: \max_{\boldsymbol{\delta},\boldsymbol{\theta},\boldsymbol{p}^{\mathrm{S}},\boldsymbol{p}^{\mathrm{A}}} \sum_{n\in\mathcal{N}'} \zeta_n(k) \tag{26}$$

$$\text{s.t. } \sum_{n\in\mathcal{N}'} \theta_{n,m}(k) \le 1, \ \forall m \in \mathcal{M}, \tag{26a}$$

Authorized licensed use limited to: University of Waterloo. Downloaded on March 04,2025 at 21:56:16 UTC from IEEE Xplore. Restrictions apply.

$$\sum_{m\in\mathcal{M}} \theta_{n,m}(k)p^{\mathrm{S}}_{n,m}(k) \le p^{\mathrm{S}}_{\max}, \quad \forall n \in \mathcal{N}', \tag{26b}$$

$$\sum_{n\in\mathcal{N}'}\sum_{m\in\mathcal{M}} \delta_n(k)\theta_{n,m}p^{\mathrm{A}}_{n,m}(k) \le p^{\mathrm{A}}_{\max}, \tag{26c}$$

$$\theta_{n,m}(k) \in \{0,1\}, \forall n \in \mathcal{N}', \forall m \in \mathcal{M}, \tag{26d}$$

$$\delta_n(k) \in \{0,1\}, \quad \forall n \in \mathcal{N}', \tag{26e}$$

where $\mathcal{N}'$ denotes the set of scheduled sensors, and the sensor $n \in \mathcal{N}'$ satisfies $\xi_n(k) = 1, \forall n \in \mathcal{N}$.

In the remainder of this section, the estimation gain-based sensor scheduling algorithm is proposed to solve $\mathcal{SP}_1$. As $\mathcal{SP}_2$ is a MINLP problem, it is decomposed into three subproblems, which are then solved in an iterative way.

A. Sensor Scheduling

The sensor subproblem $\mathcal{SP}_1$ is still non-convex due to the nonlinear objective function and the non-convex constraints ((24a), (24g), (24h)), and the objective function is the quadric form of the estimation error $\mathbf{e}(k)$. For easy to solve this problem, the estimation gain $e_{n,\Delta}(k)$ is defined as the contribution of scheduling one sensor on the estimation error reduction, which is expressed as

$$e_{n,\Delta}(k) = \|\mathbf{e}^0_n(k)\|_2^2 - \|\mathbf{e}^1(k)\|_2^2, \tag{27}$$

where $\mathbf{e}^0_n(k)$ denotes the estimation error when only the n-th sensor is not scheduled, and $\mathbf{e}^1(k)$ denotes the estimation error when all sensors are scheduled and the sensory data is successfully received by the remote estimator. Then, the sensor scheduling problem $\mathcal{SP}_1$ could be rewritten as

$$\begin{aligned} \max_{\xi} \quad & \mathrm{Tr}\left(\mathbb{E}\left\{\mathrm{diag}\left\{\xi_1(k),\ldots,\xi_N(k)\right\}\mathbf{e}_\Delta(k)\right\}\right) \\ \text{s.t.} \quad & (24a), (24g), (24h), \end{aligned} \tag{28}$$

where $\mathbf{e}_\Delta(k) = [e_{1,\Delta}(k),\ldots,e_{n,\Delta}(k),\ldots,e_{N,\Delta}(k)]^T$. It can be seen that the transformed objective function is proportional to the contribution of scheduling one sensor on the estimation error reduction, and the rewritten subproblem is a binary integer programming that could be solved optimally with the brute-force search method. Due to the exponential complexity, an estimation gain-based sensor scheduling algorithm is proposed to solve the problem (28) effectively and efficiently, shown as Algorithm 1. Firstly, the estimation gain of each sensor is calculated (Step 4-Step 10). The corresponding computational complexity is $\mathcal{O}(N)$. Secondly, the number of sensors N_{cs} whose residual energy meets the minimum residual energy requirement can be determined. Finally, when N_{cs} meets the minimal scheduling requirement, sensors with the maximum estimation gain are scheduled in sequence, and then update the estimation gain and estimation error of scheduled sensors (Step 13-Step 19). The corresponding computational complexity is $\mathcal{O}(N_{\mathrm{cs}})$. Therefore, the time complexity of Algorithm 1 is $\mathcal{O}(N + N_{\mathrm{cs}})$.

Algorithm 1: Estimation Gain-Based Sensor Scheduling Algorithm.

1: **Input**: $N_{\min}$, M, $\boldsymbol{e}(k-1)$, $\boldsymbol{E}^{\mathbf{R}}(k-1)$;
2: **Output**: The sensor scheduling $\boldsymbol{\xi}(k)$;
3: **Initialization**: The set of scheduled sensors $\mathcal{N}'$;
4: **for** Each sensor $n \in \mathcal{N}$ **do**
5: Calculate $e^0_n(k)$ and $e^1_n(k)$ according to Eq. (23);
6: Update $e_{\Delta,n}(k)$ based on Eq. (27);
7: **if** $E^{\mathrm{R}}_n(k-1) \le E^{\mathrm{R}}_{\min}$ **then**
8: $\mathcal{N} = \mathcal{N}\backslash n$, $e_{\Delta,n}(k) \leftarrow -\infty$;
9: **end if**
10: **end for**
11: $N_{\mathrm{cs}} = \min\{M, |\mathcal{N}|\}$, $\boldsymbol{e}(k) \leftarrow \boldsymbol{e}^{\mathbf{0}}(k)$;
12: **if** $N_{\mathrm{cs}} \ge N_{\min}$ **then**
13: **while** $|\mathcal{N}'| \le N_{\mathrm{cs}}$ **do**
14: $n_0 \leftarrow \arg\max_{n\in\mathcal{N}}\{e_{\Delta,n}(k)\}$;
15: $\xi_{n_0}(k) \leftarrow 1$;
16: $\mathcal{N}' \leftarrow n_0$
17: $e_{\Delta,n_0}(k) \leftarrow -\infty$;
18: $e_{n_0}(k) \leftarrow e^1_{n_0}(k)$;
19: **end while**
20: **else**
21: Break;
22: **end if**
23: **return** $\boldsymbol{\xi}(k)$;

B. Adaptive Cooperative Transmission

It is challenging to deal with $\mathcal{SP}_2$, since its objective function cannot be expressed explicitly with decision variables. In order to find a breakthrough point in solving the problem, we analyze the impact of the cardinality of the set $\mathcal{N}'$ and the amount of sensory data successfully received by RE on the objective function. First, the cardinality of the set $\mathcal{N}'$ determines the upper bound of the objective function, while the amount of sensory data successfully received by RE determines the gap from its upper bound. In particular, the cardinality of the set $\mathcal{N}'$ is limited by the number of schedulable sensors. Moreover, the more the sensors participate in data transmission, the smaller the estimation error will be. Thus, it is necessary to encourage the scheduled sensors to participate in the sensory data by enlarging the residual energy. As we all know, minimizing the transmission power of sensors is an efficient way to enlarge the residual energy. Therefore, in order to maximize the number of sensors that participate in data transmission, the energy consumption of data transmission should be reduced as much as possible. Second, the transmission status of the sensory data depends on its transmission delay according to (20). Therefore, the transmission delay constraint (i.e., $t_n(k) \le \tau$) can be used to determine the number of sensory data that are successfully received. Based on the above analysis, the problem $\mathcal{SP}_2$ can be rewritten as

$$\begin{aligned} \min_{\boldsymbol{\delta},\boldsymbol{\theta},\boldsymbol{p}^{\mathrm{S}},\boldsymbol{p}^{\mathrm{A}}} \quad & \sum_{n\in\mathcal{N}'} E^{\mathrm{T}}_n(k) \\ \text{s.t.} \quad & (26a) - (26e), \end{aligned} \tag{29}$$

Authorized licensed use limited to: University of Waterloo. Downloaded on March 04,2025 at 21:56:16 UTC from IEEE Xplore. Restrictions apply.

$$t_n(k) \le \tau, \forall n \in \mathcal{N}', \tag{29a}$$

where (29a) is the transmission delay constraint.

Theorem 1: $E_n^{\mathrm{T}}(k)$ is a monotonically increasing function of the $p_{n,m}^{\mathrm{S}}(k)$.

Proof: Proof is shown in Appendix A.

Based on Theorem 1, the problem (29) can be transformed into

$$\min_{\boldsymbol{\delta},\boldsymbol{\theta},\boldsymbol{p}^{\mathbf{S}},\boldsymbol{p}^{\mathbf{A}}} \quad \sum_{n\in\mathcal{N}'}\sum_{m\in\mathcal{M}} \theta_{n,m}(k) p_{n,m}^{\mathrm{S}}(k)$$
$$\text{s.t.} \quad (26a)-(26e), (29a), \tag{30}$$

where the objective function is the linear combination of decision variables, but the non-convex constraint (29a) poses significant challenges to solving problem (30). In order to tackle the non-convex problem (30) efficiently, a joint optimization algorithm of mode selection, subcarrier allocation and power control is proposed to iteratively solve the this problem.

1) Mode Selection: When the subcarrier allocation $\boldsymbol{\theta}$ and transmit power $(\boldsymbol{p}^{\mathbf{S}}, \boldsymbol{p}^{\mathbf{A}})$ are given, the sensor will select a transmission mode that could achieve a larger transmission rate. Then, the optimal mode selection could be determined by

$$\delta_n(k) = \begin{cases} 1, & \text{if } R^{\mathrm{C}_n(k)} > R_n^{\mathrm{D}}(k), \quad \forall n \in \mathcal{N}', \\ 0, & \text{otherwise.} \end{cases} \tag{31}$$

2) Subcarrier Allocation: When the transmission mode selection $\boldsymbol{\delta}$ and transmit power $(\boldsymbol{p}^{\mathbf{S}}, \boldsymbol{p}^{\mathbf{A}})$ are given, the achievable transmission rate is only affected by the subcarrier allocation strategy. For ease of representation, the variable $\omega_{n,m}(k)$ is introduced to evaluate the achievable transmission rate utility under different subcarrier allocations, shown as below.

$$\omega_{n,m}(k) = \omega_0 e_{\Delta,n}(k) \Big((1-\delta_n(k)) \left(R_n^{\mathrm{D}}(k) - R_n^{\min}(k)\right) + \delta_n(k) \left(R_n^{\mathrm{C}}(k) - R_n^{\min}(k)\right) \Big), \forall n \in \mathcal{N}', \tag{32}$$

where ω_0 is the penalty factor that is introduced to avoid the transmission rate being less than the minimization value; $R_n^{\min}(k) = q_n(k)/\tau$. Then, the subproblem of subcarrier allocation can be rewritten as

$$\max_{\boldsymbol{\theta}} \quad \sum_{n\in\mathcal{N}'}\sum_{m\in\mathcal{M}} \theta_{n,m}(k)\omega_{n,m}(k)$$
$$\text{s.t.} \quad (26a), (26d). \tag{33}$$

The problem (33) is a binary linear programming problem, which could be optimally solved with the exhaustive search approach at the cost of exponential complexity. In this work, the problem is efficiently solved by reformulating it as a weighted bipartite graph matching problem. Generally, a weighted bipartite graph is defined as $\mathbb{G}(\mathcal{V}, \mathcal{E}, \mathcal{W})$. The set of vertices is denoted as $\mathcal{V} = \mathcal{N}' \cup \mathcal{M}$. Moreover, $\mathcal{E}$ is the set of edges connecting a vertex in $\mathcal{N}'$ and a vertex in $\mathcal{M}$. The weight of edges is denoted as the vector $\mathcal{W}$. In this work, the weight of the line connecting the n-th vertex and the m-th vertex is set as $\omega_{n,m}(k)$. The Kuhn-Munkres (KM) algorithm is an efficient method to solve the binary weighted matching problem [42]. The KM theorem transforms the weighted matching problem into a combinatorial one of finding a perfect matching [43]. Note that KM algorithm could obtain the optimal solution, only when the number of nodes in $\mathcal{N}'$ is equal to that in $\mathcal{M}$. Specially, when $|\mathcal{N}'| = M$, the original maximum weight matching problem is a perfect matching problem, and the optimal matching obtained with the KM algorithm is the optimal solution of the original maximum weight matching problem. When $|\mathcal{N}'| < M$, although it can be transformed into a perfect matching problem by adding dummy nodes to the $\mathcal{N}'$, the optimal matching found by the KM algorithm is not the optimal solution to the original maximum weight matching problem. The reason is that the subcarriers matched to the dummy nodes in fact are not allocated to any sensors for data transmission. Therefore, the subcarriers matched to the dummy nodes need to be reallocated to improve the transmission rate. To achieve this goal, an algorithm based on the KM theorem is designed to determine the allocation relationship between sensors and subcarriers, as shown in Algorithm 2.

The main idea of Algorithm 2 is to allocate subcarriers among sensors to the following steps. In particular, the weights of each edge in the matching matrix are calculated (Step 4-Step 7). The corresponding computational complexity is $\mathcal{O}(|\mathcal{N}'|M)$. Then, when $|\mathcal{N}'| = M$, the optimal subcarrier allocation can be obtained directly by the KM algorithm (Step 10-Step 12). The corresponding computational complexity is $\mathcal{O}(M^3)$. When $|\mathcal{N}'| < M$, $M - |\mathcal{N}'|$ dummy nodes are added to the set $\mathcal{N}'$ to the dimension of $\mathcal{N}'$ is equal to that of $\mathcal{M}$. Then, the edges between each dummy node in $\mathcal{N}'$ and any node in $\mathcal{M}$ are added, whose weight is set to be zero. Moreover, the subcarrier matched to the dummy node is added to the subcarrier candidate set. Next, the subcarriers in the candidate set are matched to the sensors in $\mathcal{N}'$, and calculate the rate utility gap between unallocated subcarriers and allocated subcarriers. Finally, the subcarrier is allocated to the sensor with the largest rate utility gap (Step 15-Step 37). The corresponding computational complexity is $\mathcal{O}(M^3)$. The original maximum weight matching problem is solved until the candidate set is null. Therefore, the time complexity of Algorithm 2 is $\mathcal{O}(|\mathcal{N}'|M + M^3)$.

3) Power Control: According to the constraint (29a), it can be seen that the problem formulations of power control are different in different transmission modes. Therefore, we study the power optimization schemes under the direct transmission mode and the cooperative transmission mode, respectively.

a) Direct transmission mode: In this case, $\delta_n(k) = 0, \forall n \in \mathcal{N}'$. The subproblem of power control is given by

$$\min_{\boldsymbol{p}^{\mathbf{S}}} \quad \sum_{n\in\mathcal{N}'}\sum_{m\in\mathcal{M}} \theta_{n,m}(k) p_{n,m}^{\mathrm{S}}(k) \tag{34}$$
$$\text{s.t.} \quad (26b),$$
$$R_n^{\mathrm{D}}(k) \ge R_n^{\min}(k), \forall n \in \mathcal{N}', \tag{34a}$$

which is convex problem due to the linear objective function and the convex constraints (26b) and (34a). Therefore, it can be solved by a standard convex optimization solver (such as cvxpy).

Authorized licensed use limited to: University of Waterloo. Downloaded on March 04,2025 at 21:56:16 UTC from IEEE Xplore. Restrictions apply.

b) Cooperative transmission mode: In this case, $\delta_n(k) = 1, \forall n \in \mathcal{N}'$. The subproblem formulation is expressed as

$$\min_{\boldsymbol{p}^{\mathbf{S}},\boldsymbol{p}^{\mathbf{A}}} \sum_{n\in\mathcal{N}''}\sum_{m\in\mathcal{M}} \theta_{n,m}(k)p^{\mathrm{S}}_{n,m}(k) \tag{35}$$

$$\text{s.t.} \sum_{m\in\mathcal{M}} \theta_{n,m}(k)p^{\mathrm{S}}_{n,m}(k) \le p^{\mathrm{S}}_{\max}, \forall n \in \mathcal{N}'', \tag{35a}$$

$$\sum_{n\in\mathcal{N}''}\sum_{m\in\mathcal{M}} \theta_{n,m}(k)p^{\mathrm{A}}_{n,m}(k) \le p^{\mathrm{A}}_{max}, \tag{35b}$$

$$R^{\mathrm{C}}_n(k) \ge R^{\min}_n(k), \ \forall n \in \mathcal{N}'', \tag{35c}$$

where $\mathcal{N}''$ is the set of scheduled sensors in the cooperative transmission mode. Constraint (35c) is concave since its Hessian matrix is negative semi-definite [44]. Moreover, $\boldsymbol{p}^{\mathbf{S}}$ and $\boldsymbol{p}^{\mathbf{A}}$ in constraint (35c) is tightly coupled. Therefore, (35) is concave problem and cannot be efficiently solved with existing methods. In this work, the Lagrangian method is employed to solve this problem. The Lagrangian function of (35) is shown as (38), shown at the bottom of this page, where $\boldsymbol{\lambda}^{\mathbf{S}}$, λ^{A}, and $\boldsymbol{\lambda}^{\mathbf{R}}$ are the non-negative Lagrangian multipliers. According to the Karush-Kuhn-Tucker conditions, the optimal solution to (35) could be obtained by letting the gradient be zero, shown as

$$\frac{\partial L\left(\lambda^{\mathrm{S}}_n,\lambda^{\mathrm{A}},\lambda^{\mathrm{R}}_n,p^{\mathrm{S}}_{n,m}(k),p^{\mathrm{A}}_{n,m}(k)\right)}{\partial p^{\mathrm{S}}_{n,m}(k)} = 0\Bigg|_{p^{\mathrm{S}}_{n,m}(k)=p^{*,\mathrm{S}}_{n,m}(k)}, \tag{36}$$

$$\frac{\partial L\left(\lambda^{\mathrm{S}}_n,\lambda^{\mathrm{A}},\lambda^{\mathrm{R}}_n,p^{\mathrm{S}}_{n,m}(k),p^{\mathrm{A}}_{n,m}(k)\right)}{\partial p^{\mathrm{A}}_{n,m}(k)} = 0\Bigg|_{p^{\mathrm{A}}_{n,m}(k)=p^{*,\mathrm{A}}_{n,m}(k)}. \tag{37}$$

The optimal power of the n-th sensor is expressed as (39), shown at the bottom of this page, The optimal power at the n-th sensor relayed by the AGV is given by

$$p^{*,\mathrm{A}}_{n,m}(k) = \gamma^{\mathrm{SA}}_{n,m}(k)\Psi_{n,m}p^{*,\mathrm{S}}_{n,m}(k), \tag{43}$$

where $\Psi_{n,m}$ is expressed as (40), shown at the bottom of this page. Note that $[x]^+ = \max(0, x)$. The details of the derivation of (39) and (43) can be described in the following steps. Firstly, from (36) and (37), one can respectively obtain (41) and (42), shown at the bottom of this page. Secondly, by dividing (41) and (42) one can relate $p^{*,\mathrm{A}}_{n,m}(k)$ and $p^{*,\mathrm{S}}_{n,m}(k)$ as in (43). Finally, by substituting (43) into (42), one can obtain the optimal power of n-th sensor at k-th estimation step on m-th subcarrier as in (39).

Equations (39) and (43) give a unique solution to the optimization problem (35), hence, the optimal solution of this problem can be obtained with the Lagrangian method. The update of Lagrangian multipliers is given by

$$\begin{aligned}\lambda^{\mathrm{S}}_n(t+1) &= \lambda^{\mathrm{S}}_n(t) - \alpha^{\mathrm{S}}(t)\left(p^{\mathrm{S}}_{\max} - \sum_{m\in\mathcal{M}}\theta_{n,m}(k)p^{\mathrm{S}}_{n,m}(k)\right),\\ \lambda^{\mathrm{A}}(t+1) &= \lambda^{\mathrm{A}}(t)\end{aligned} \tag{44}$$

$$L\left(\lambda^{\mathrm{S}}_n,\lambda^{\mathrm{A}},\lambda^{\mathrm{R}}_n,p^{\mathrm{S}}_{n,m}(k),p^{\mathrm{A}}_{n,m}(k)\right) = \sum_{n\in\mathcal{N}''}\sum_{m\in\mathcal{M}}\theta_{n,m}(k)p^{\mathrm{S}}_{n,m}(k) + \lambda^{\mathrm{S}}_n\left(\sum_{m\in\mathcal{M}}\theta_{n,m}(k)p^{\mathrm{S}}_{n,m}(k) - p^{\mathrm{S}}_{\max}\right) + \lambda^{\mathrm{A}}\left(\sum_{n\in\mathcal{N}''}\sum_{m\in\mathcal{M}}\theta_{n,m}(k)p^{\mathrm{A}}_{n,m}(k) - p^{\mathrm{A}}_{\max}\right) + \lambda^{\mathrm{R}}_n\left(R^{\min}_n(k) - R^{\mathrm{C}}_n(k)\right), \tag{38}$$

$$p^{*,\mathrm{S}}_{n,m}(k) = \left[\frac{\frac{\lambda^{\mathrm{R}}_n\gamma^{\mathrm{AR}}_{n,m}(k)}{2B\ln(2)(1+\lambda^{\mathrm{A}})} - \left(1+\gamma^{\mathrm{AR}}_{n,m}(k)\Psi_{n,m}\right)^2}{\gamma^{\mathrm{SR}}_{n,m}(k)\left(1+\gamma^{\mathrm{AR}}_{n,m}(k)\Psi_{n,m}\right)^2 + \gamma^{\mathrm{SA}}_{n,m}(k)\gamma^{\mathrm{AR}}_{n,m}(k)\Psi_{n,m}\left(1+\gamma^{\mathrm{AR}}_{n,m}(k)\Psi_{n,m}\right)}\right]^+, \tag{39}$$

$$\Psi_{n,m} = \frac{\sqrt{\left(\gamma^{\mathrm{SR}}_{n,m}(k)\gamma^{\mathrm{AR}}_{n,m}(k) + \gamma^{\mathrm{SA}}_{n,m}(k)\gamma^{\mathrm{AR}}_{n,m}(k)\right)\left(1+\lambda^{\mathrm{S}}_n\right) - \gamma^{\mathrm{SR}}_{n,m}(k)\gamma^{\mathrm{SA}}_{n,m}(k)\lambda^{\mathrm{A}}} - \gamma^{\mathrm{SR}}_{n,m}(k)}{\gamma^{\mathrm{SR}}_{n,m}(k)\gamma^{\mathrm{AR}}_{n,m}(k) + \gamma^{\mathrm{SA}}_{n,m}(k)\gamma^{\mathrm{AR}}_{n,m}(k)}. \tag{40}$$

$$\begin{aligned}&\frac{1}{1+\lambda^{\mathrm{S}}_n}\left(\gamma^{\mathrm{SR}}_{n,m}(k)\left(p^{\mathrm{S}}_{n,m}(k)\gamma^{\mathrm{SA}}_{n,m}(k) + p^{\mathrm{A}}_{n,m}(k)\gamma^{\mathrm{AR}}_{n,m}(k)\right)^2 + p^{2,\mathrm{A}}_{n,m}(k)\gamma^{\mathrm{SA}}_{n,m}(k)\gamma^{2,\mathrm{AR}}_{n,m}(k)\right)\\ &= \frac{2\ln(2)}{B\lambda^{\mathrm{R}}_n}\left(1 + p^{\mathrm{S}}_{n,m}(k)\gamma^{\mathrm{SR}}_{n,m}(k) + \frac{p^{\mathrm{S}}_{n,m}(k)\gamma^{\mathrm{SA}}_{n,m}(k)p^{\mathrm{A}}_{n,m}(k)\gamma^{\mathrm{AR}}_{n,m}(k)}{p^{\mathrm{S}}_{n,m}(k)\gamma^{\mathrm{SA}}_{n,m}(k) + p^{\mathrm{A}}_{n,m}(k)\gamma^{\mathrm{AR}}_{n,m}(k)}\right)\left(p^{\mathrm{S}}_{n,m}(k)\gamma^{\mathrm{SA}}_{n,m}(k) + p^{\mathrm{A}}_{n,m}(k)\gamma^{\mathrm{AR}}_{n,m}(k)\right)^2,\end{aligned} \tag{41}$$

$$\begin{aligned}&\frac{1}{\lambda^{\mathrm{A}}_n}p^{2,\mathrm{S}}_{n,m}(k)\gamma^{2,\mathrm{SA}}_{n,m}(k)\gamma^{\mathrm{AR}}_{n,m}(k)\\ &= \frac{2\ln(2)}{B\lambda^{\mathrm{R}}_n}\left(1 + p^{\mathrm{S}}_{n,m}(k)\gamma^{\mathrm{SR}}_{n,m}(k) + \frac{p^{\mathrm{S}}_{n,m}(k)\gamma^{\mathrm{SA}}_{n,m}(k)p^{\mathrm{A}}_{n,m}(k)\gamma^{\mathrm{AR}}_{n,m}(k)}{p^{\mathrm{S}}_{n,m}(k)\gamma^{\mathrm{SA}}_{n,m}(k) + p^{\mathrm{A}}_{n,m}(k)\gamma^{\mathrm{AR}}_{n,m}(k)}\right)\left(p^{\mathrm{S}}_{n,m}(k)\gamma^{\mathrm{SA}}_{n,m}(k) + p^{\mathrm{A}}_{n,m}(k)\gamma^{\mathrm{AR}}_{n,m}(k)\right)^2.\end{aligned} \tag{42}$$

Authorized licensed use limited to: University of Waterloo. Downloaded on March 04,2025 at 21:56:16 UTC from IEEE Xplore. Restrictions apply.

Algorithm 2: Subcarrier Allocation Algorithm.

Input: $\mathcal{N}'$, $\mathcal{M}$, $\boldsymbol{\delta}(k)$, $\boldsymbol{p}^{\mathbf{S}}(k)$, $\boldsymbol{p}^{\mathbf{A}}(k)$;
Output: The subcarrier allocation $\boldsymbol{\theta}(k)$;
Initialization: $\boldsymbol{\Omega} = \varnothing$;
for Each sensor $n \in \mathcal{N}'$ **do**
  for Each subcarrier $m \in \mathcal{M}$ **do**
    Calculate the weight $\Omega_{n,m} = \omega_{n,m}(k)$ according to Eq. (32);
  end for
end for
$N_{\mathrm{s}} \leftarrow |\mathcal{N}'|$;
if $N_{\mathrm{s}} = M$ **then**
  Obtain optimal subcarrier allocation $\boldsymbol{\theta}(k)$ by KM algorithm;
  Break;
else
  $d \leftarrow 0$;
  while $N_{\mathrm{s}} + d + 1 \leq M$ **do**
    for Each subcarrier $m \in \mathcal{M}$ **do**
      $\Omega_{N_{\mathrm{s}}+d+1,m} = 0$;
    end for
    $d \leftarrow d + 1$;
  end while
  Obtain subcarrier allocation $\boldsymbol{\theta}(k)$ by KM algorithm;
  for Each sensor $n \in \mathcal{N}'$ **do**
    $\mathcal{M}_n \leftarrow m | \theta_{n,m} == 1$;
    $\mathcal{M} = \mathcal{M} \backslash \mathcal{M}_n$;
    $\Omega_n^0 \leftarrow \sum_{m \in \mathcal{M}_n} \omega_{n,m}(k)$;
  end for
  for Each subcarrier $m \in \mathcal{M}$ **do**
    for Each sensor $n \in \mathcal{N}'$ **do**
      $\mathcal{M}' \leftarrow \mathcal{M}_n \cup m$;
      $\Omega_n^1 \leftarrow \sum_{m' \in \mathcal{M}'} \omega_{n,m'}(k)$;
      $\Omega_{\Delta,n} \leftarrow \Omega_n^1 - \Omega_n^0$;
    end for
    $n' \leftarrow \arg\max_{n \in \mathcal{N}'} \{\Omega_{\Delta,n}\}$;
    $\theta_{n',m}(k) \leftarrow 1$;
    $\mathcal{M}_{n'} \leftarrow \mathcal{M}_{n'} \cup m$;
    $\Omega_{n'}^0 \leftarrow \Omega_{n'}^1$;
  end for
end if
return $\boldsymbol{\theta}(k)$;

Algorithm 3: Adaptive Cooperative Transmission Algorithm.

Input: $\mathcal{N}'$, $\mathcal{M}$;
Output: $\boldsymbol{\delta}(k)$, $\boldsymbol{\theta}(k)$, $\boldsymbol{p}^{\mathbf{S}}(k)$, $\boldsymbol{p}^{\mathbf{A}}(k)$;
Initialization: $t = 0$, $T = 0$, $fit(t) = 0$, $Fit(T) = 0$, $\boldsymbol{\lambda}^{\mathbf{S}}(t)$, $\lambda^{\mathrm{A}}(t)$, $\boldsymbol{\lambda}^{\mathbf{R}}(t)$;
while $T \leq T_{\max}$ **do**
  for Each sensor $n \in \mathcal{N}'$ **do**
    Update $\delta_n(k)$ according to (31);
  end for
  Update $\boldsymbol{\theta}(k)$ according to Algorithm (2);
  for Each sensor $n \in \mathcal{N}'$ **do**
    Calculate the maximum achievable transmission rate $R_n^{\max}$, where the transmit power is $p_{\max}^{\mathrm{S}}$;
    if $R_n^{\max} < R_n^{\min}(k)$ **then**
      $\mathcal{N}' = \mathcal{N}' \backslash n$, $p_n^{\mathrm{S}}(k) \leftarrow p_{\max}^{\mathrm{S}}$;
      $e_n(k) \leftarrow e_n^0(k)$;
    end if
  end for
  for Each sensor $n \in \mathcal{N}'$ **do**
    if $\boldsymbol{\delta}(k) = 0$ **then**
      Calculate $p_{n,m}^{\mathrm{S}}(k)$ based on (34);
    else
      $\mathcal{N}'' \leftarrow n | \delta_n(k) == 1$;
    end if
  end for
  while $t \leq t_{\max}$ **do**
    $t \leftarrow t + 1$;
    Update $\boldsymbol{\lambda}^{\mathbf{S}}(t)$, $\lambda^{\mathrm{A}}(t)$ and $\boldsymbol{\lambda}^{\mathbf{R}}(t)$ according to Eq. (44), (45) and (46), respectively;
    Update $\boldsymbol{p}^{*,\mathbf{S}}(k)$ and $\boldsymbol{p}^{*,\mathbf{A}}(k)$ according to Eq. (39) and Eq. (43), respectively;
    $fit(t) \leftarrow \sum_{n \in \mathcal{N}''} \sum_{m \in \mathcal{M}} \theta_{n,m}(k) p_{n,m}^{*,\mathrm{S}}(k)$;
    if $fit(t) - fit(t-1) < \epsilon$ **then**
      $Fit(T) \leftarrow fit(t)$;
      Break;
    end if
  end while
  if $Fit(T) - Fit(T-1) < \epsilon$ **then**
    Break;
  end if
end while
Update remaining energy $\boldsymbol{E}^{\mathbf{R}}(k)$ according to Eq. (16);
return $\boldsymbol{\delta}(k)$, $\boldsymbol{\theta}(k)$, $\boldsymbol{p}^{\mathbf{S}}(k)$, $\boldsymbol{p}^{\mathbf{A}}(k)$;

$$- \alpha^{\mathrm{A}}(t) \left(p_{\max}^{\mathrm{A}} - \sum_{n \in \mathcal{N}''} \sum_{m \in \mathcal{M}} \theta_{n,m}(k) p_{n,m}^{\mathrm{A}}(k) \right), \tag{45}$$

$$\lambda_n^{\mathrm{R}}(t+1) = \lambda_n^{\mathrm{R}}(t) - \alpha^{\mathrm{R}}(t) \left(R_n^{\mathrm{C}}(k) - R_n^{\min}(k) \right), \tag{46}$$

where $\alpha^{\mathrm{S}}(t)$, $\alpha^{\mathrm{A}}(t)$ and $\alpha^{\mathrm{R}}(t)$ are sufficiently small step and t is the iteration index.

The detailed solution procedure of $\mathcal{SP}_2$ is shown as Algorithm 3. Specifically, in each iteration, the transmission mode of the scheduled sensors is firstly determined (Step 5-Step 7). The corresponding computational complexity is $\mathcal{O}(|\mathcal{N}'|)$. Then, the subcarrier allocation is determined with Algorithm 2 (Step 8). The corresponding computational complexity is $\mathcal{O}(|\mathcal{N}'|M + M^3)$. Subsequently, check whether the requirement of minimum transmission rate is met. If not, the transmit power of the sensor will not be optimized, and the estimated error value will be returned (Step 9-Step 15). The corresponding computational complexity is $\mathcal{O}(|\mathcal{N}'|)$. Next, the sensor transmit power under the direct transmission mode is solved by a standard convex optimization solver, and the sensor transmit power under the cooperative transmission mode is iteratively solved by the

Authorized licensed use limited to: University of Waterloo. Downloaded on March 04,2025 at 21:56:16 UTC from IEEE Xplore. Restrictions apply.

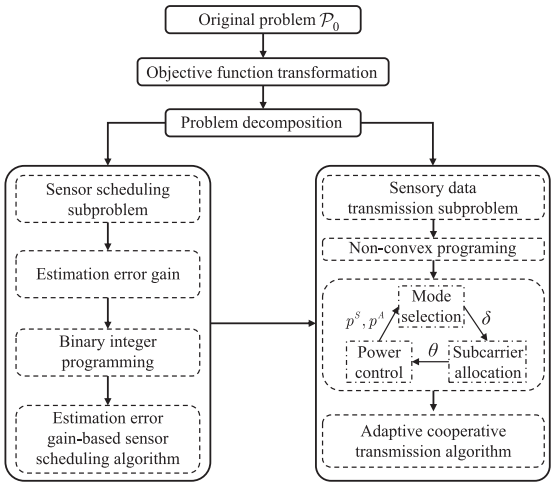

Fig. 3. The diagram of solution process.

Lagrangian method (Step 16-Step 32). To simplify the analysis, we assume that the number of iterations of Algorithm 3 is Φ and the number of iterations of the Lagrangian method is ϕ. Therefore, the computational complexity of Algorithm 3 is $\mathcal{O}(\Phi(3|\mathcal{N}'| + |\mathcal{N}'|M + M^3 + \phi))$.

In summary, the original problem is a MINLP problem, whose optimal solution is difficult to obtain. As a solution, the original problem is divided into two subproblems, namely the sensor scheduling subproblem and the sensory data transmission subproblem. Both subproblems are non-convex problems. The former one is transformed into a binary integer programming problem based on the proposed estimation gain index. The transformed problem then can be optimally solved with the designed Algorithm 1. The latter one contains non-convex constraints, which is decomposed into three subproblems and then solved with an iterative method. The detailed solution process is shown as Fig. 3. Subsequently, we will discuss the solvability and optimality of each subproblem. The sensor scheduling subproblem is transformed into a binary integer programming problem based on the proposed estimation gain index. Then, the transformed problem could be optimally solved with the designed Algorithm 1 in the revised manuscript. Thus, the sensor scheduling subproblem is solvable and could be solved optimally with designed algorithm. The sensory data transmission subproblem is decomposed into three subproblems and solved in an iterative manner. The convergence of the iterative process is show in Fig. 4. It can be seen that the solution process is convergent after about 1000 iterations. Therefore, the sensory data transmission subproblem is solvable. As the iterative process is converged to 0.018 rather than zero, the solution of sensory data transmission subproblem obtained with the designed iterative algorithm is near-optimal. In summary, solvability can be guaranteed, but optimality can not.

IV. Performance Evaluation

In this paper, the proposed adaptive cooperative transmission (ACT) scheme jointly designs the sensory data transmission and sensor scheduling for state estimation to enhance the accuracy of state estimation in the AGV-assisted industrial IoT system.

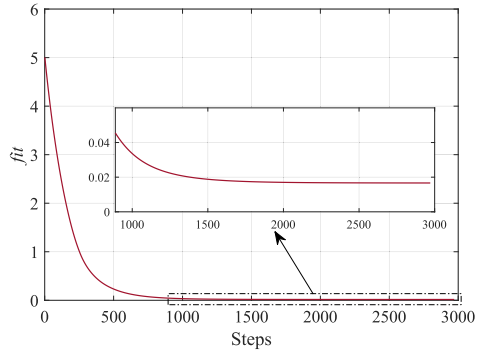

Fig. 4. The convergence of the iterative solution process for the sensory data transmission subproblem.

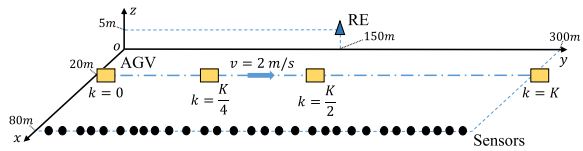

Fig. 5. Network topology.

In this section, we perform extensive simulations to evaluate the performance of ACT scheme in terms of mean square error, energy consumption and transmission success rate. The transmission success rate is defined as the ratio of the number of sensors whose sensory data is not successfully received by CE to the number of scheduled sensors. Four additional schemes are considered as comparing ones. The first one is the direct transmission and sensor scheduling (DTSS) scheme, where all the scheduled sensors select the direct transmission mode. The second one is an adaptive cooperative transmission with random scheduling (ACTRS) scheme, in which the scheduled sensors in each estimation step are randomly generated. The third one is an adaptive cooperative transmission scheme based on random subcarrier allocation (ACT-RSA), in which subcarriers are randomly assigned to the scheduled sensors without considering subcarrier allocation optimization. The fourth one is an adaptive cooperative transmission scheme based on maximum transmit power (ACT-MTP), in which the scheduled sensors transmit sensory data at maximum transmit power.

The performance comparison is evaluated according to the network topology covering a rectangular area $[0, 80]_{\mathrm{m}} \times [0, 300]_{\mathrm{m}}$, where $N = 30$ sensors are placed, the antenna height of the AGV is $H_{\mathrm{A}} = 1.5$ m and the RE is placed at the horizontal center of the network whose height is $H_{\mathrm{R}} = 5$ m, as shown in Fig. 5. Moreover, the initial residual energy of the sensor is $\boldsymbol{E}^{\mathbf{R}}(0) = 100$ mJ, $E_0^{\mathrm{D}} = 0.1$ mJ/s. The main parameters used in the simulation are shown in Table I. The computer is built on the Windows 10 with Intel Core 3.40GHz i5-12500 CPU and 16GB of RAM. According to simulation settings, the running time of proposed algorithm is about 15 ms. Based on the running result, the transmission duration of one data packet is about 70ms. Then, the total duration of data transmission and algorithm running is 85 ms, which is less than the duration of estimation step. Therefore, the timeliness requirement of state estimation in control systems could be satisfied.

Authorized licensed use limited to: University of Waterloo. Downloaded on March 04,2025 at 21:56:16 UTC from IEEE Xplore. Restrictions apply.

TABLE I
MAIN PARAMETERS

Parameters	Values
Corner distance $[D_0, D_1, D_2, D_3]$	$[0, 50, 110, \infty]$
Pathloss exponents $[\beta_0, \beta_1, \beta_2]$	$[2.8, 3.4, 4]$
Noise power σ^2	-42 dBm
Bandwidth of each subcarrier B	180 kHz
The duration of one estimation step τ	100 ms
Average packet length of the sensory data	2 Kbits
Minimum number of sensors to be scheduled $N_{\min}$	8
Number of subcarriers M	12
Maximum transmit power of sensor	10 dBm
Maximum transmit power of AGV	20 dBm

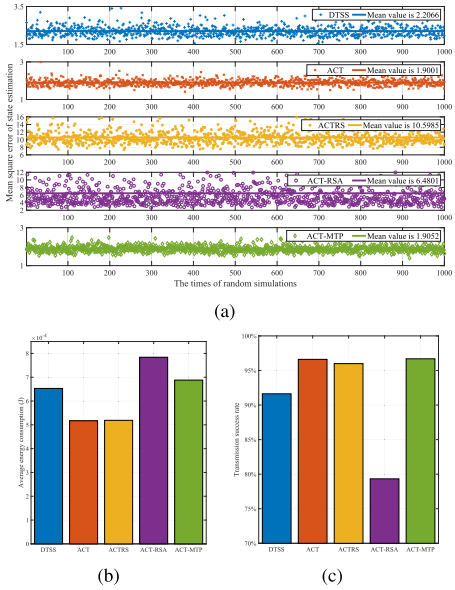

Fig. 6. Performance comparison among different approaches. (a) Mean square estimation error. (b) Average energy consumption. (c) Transmission success rate.

A. Performance Comparison With Different Schemes

The performance comparison among five compared ones terms of mean square estimation error, average energy consumption, and transmission success rate is shown in Fig. 6. It can be seen that DTSS scheme performs worse than ACT scheme in terms of mean square estimation error, average energy consumption, and transmission success rate. Moreover, the mean square estimation errors of ACTRS and ACT-RSA schemes are much larger than that of the other three schemes as shown in Fig. 6(a). In addition, as shown in Fig. 6(c), ACT-RSA scheme has a minimum transmission success rate, less than 80%, while the other four schemes have a transmission success rate greater than 90%. The reason is that ACT-RSA scheme adopts a random subcarrier allocation strategy, making it difficult for sensors to obtain satisfied subcarriers, leading to a significant decrease in the data transmission success rate. The low transmission success rate of ACT-RSA scheme makes some of scheduled sensors transmit sensory data at the maximum transmit power, which causes the average energy consumption of ACT-RSA scheme larger than that of other four schemes, as shown in Fig. 6(b). Fig. 6(a) and (c) show that although the mean square estimation errors of both ACTRS and ACT-RSA schemes are relatively large, the transmission success rate of ACTRS scheme is much larger than that of ACT-RSA scheme. The reason is that ACTRS scheme results in a large mean square estimation error due to its random scheduling of sensors. Furthermore, ACT-RSA scheme leads to a decrease in the transmission success rate due to the random subcarrier allocation, consequently leading to an increase in the mean square estimation error. The above simulation results verify that the mean square estimation error is influenced by both sensor scheduling and transmission status of sensory data. It also demonstrates the superiority of the joint optimization of sensor scheduling and data transmission in ACT scheme for the considered industrial IoT system.

B. Performance Comparison With Different Parameters

The impact of average packet length on performance is shown in Fig. 7. It can be seen that the mean square estimation error and the average energy consumption of all schemes increase with the growth of the average packet length, while the transmission success rate gradually decreases. Moreover, we find that there is a critical point in the average data packet length. If the average packet length is less than this critical point, the increment mean square estimation error is small and the mean square error changed gradually flattened. However, if the average packet length is larger than this critical point, the mean square estimation error increases significantly, especially in DTSS scheme, as shown in Fig. 7(a). The reason is that with the growth of average packet length, some sensors located at the edge are constrained by transmission distance, which makes the data transmitted by these sensors unable to be successfully received by RE within the one estimation step. Even though the optimal transmission resources are allocated to these sensors, thus leading to a significant increase in the mean square estimation error. In addition, with the adaptive cooperative transmission scheme, the scheduled sensors can adaptively choose cooperative transmission or direct transmission according to the transmission conditions. Due to the mobility of AGV, the number of edge sensors whose transmitted data cannot be successfully received by RE can be effectively reduced. Therefore, the increase of mean square estimation error with ACT scheme is much smaller than that with DTSS scheme.

As shown in Fig. 7(b), when the average packet length is small, the average energy consumption of DTSS scheme is almost equal to that of ACT scheme. However, as the average packet length increases, the average energy consumption of DTSS scheme increases significantly and gradually exceeds that of ACT-MTP and ACT-RSA schemes. Therefore, ACT scheme has a significant advantage over DTSS scheme on reducing energy consumption during large data packet transmission. As shown in Fig. 7(c), ACT-RSA scheme has a much lower transmission success rate than ACT scheme due to its random subcarrier allocation. In addition, the transmission success rate of DTSS scheme decreases significantly with the increase of the average packet length, about 40%. In contrast, the transmission success rate of ACT scheme is consistently greater than that of DTSS scheme, especially when the average packet length is large. This indicates that ACT scheme is more resilient when the packet

Authorized licensed use limited to: University of Waterloo. Downloaded on March 04,2025 at 21:56:16 UTC from IEEE Xplore. Restrictions apply.

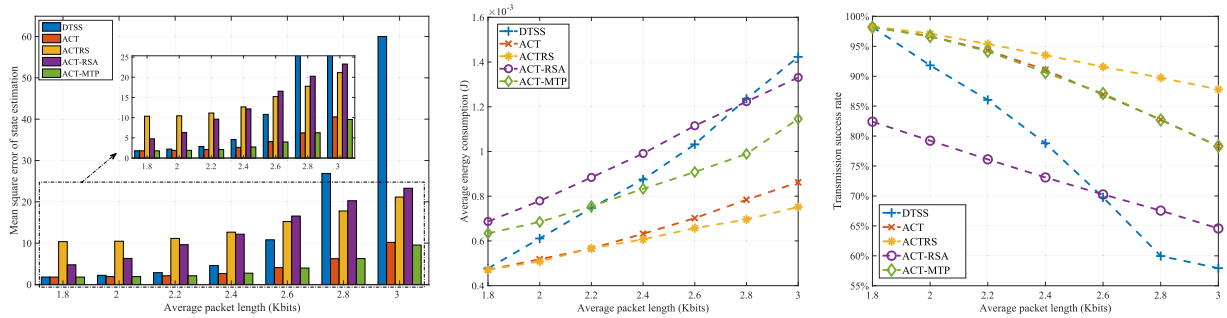

Fig. 7. Performance comparison of different average packet lengths. (a) Mean square estimation error. (b) Average energy consumption. (c) Transmission success rate.

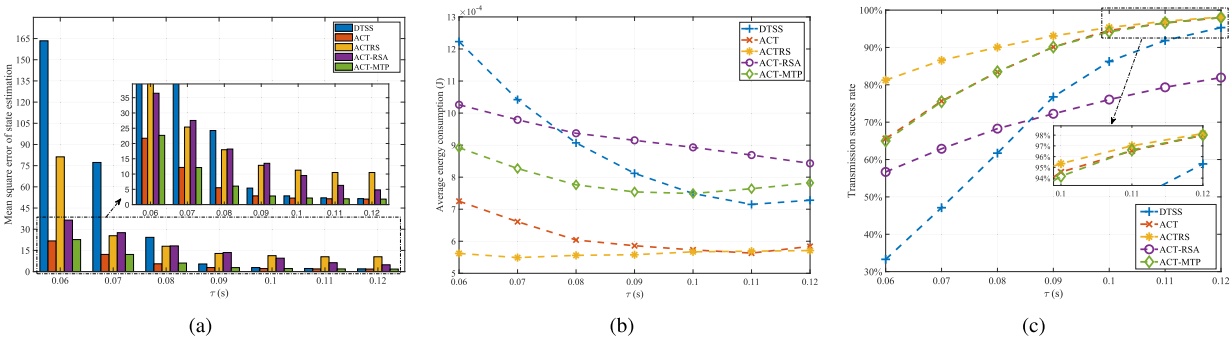

Fig. 8. Performance comparison of different duration of one estimation step. Here, the average packet length is 2.2 Kbits. (a) Mean square estimation error. (b) Average energy consumption. (c) Transmission success rate.

length increases, which can effectively delay the degradation of the transmission success rate and then ensure the performance of state estimation.

The effect of the duration of one estimation step on the performance is shown in Fig. 8. It can be seen that with the increase of the duration of one estimation step, the mean square estimation error first drops sharply and then gradually remains flat, as shown in Fig. 8(a). Moreover, with the increase of the duration, the mean square estimation error of DTSS scheme decreases significantly and is smaller than that of ACTRS and ACT-RSA schemes. In addition, when the duration is small, the mean square estimation error of DTSS scheme is much larger than that of ACT scheme (about 8 times). Therefore, compared with DTSS scheme, ACT scheme could significantly improves the estimation performance for industrial IoT systems with strict requirements on the duration of one estimation step.

As shown in Fig. 8(b), the average energy consumption of ACT-RSA scheme decreases linearly with the increase of the duration of one estimation step, while the average energy consumption of other four schemes decreases first and then increases with the increase of the duration of one estimation step. The reason is that with the increase of the duration of one estimation step, the number of sensors whose sensory data cannot be successfully received by RE within the one estimation step decreases, leading to a decrease in the average energy consumption. With the further increase of the duration, the transmission duration of all scheduled sensors is extended, so that the average energy consumption increases. As shown in Fig. 8(c), DTSS scheme has the lowest transmission success rate when the duration of one estimation step is small. With the duration increase, transmission success rate with the increase of the duration increases rapidly and exceeds ACT-RSA scheme, but it is still smaller than that with ACT scheme.

The impact of the number of subcarriers on performance is shown in Fig. 9. With the increase of the number of subcarriers, the number of sensors that can be scheduled in one estimation step increases. Therefore, the mean square estimation error decreases with the increase of the number of subcarriers, as shown in Fig. 9(a). Moreover, ACTRS has a much larger mean square estimation error than other four schemes due to its random sensor scheduling scheme. As shown in Fig. 9(b), the average energy consumption of ACT-RSA scheme gradually decreases with the increase in the number of subcarriers, while the average energy consumption of other four schemes first decreases, then increases slightly and gradually remains constant. As shown in Fig. 9(c), the transmission success rate of all schemes gradually increases with the growth in the number of subcarriers. The reason is that the probability of sensors allocated to the satisfied subcarriers increases with the growth of the number of available subcarriers, leading to an increase in the transmission success rate. The increase in the transmission success rate reduces the number of sensors transmitting data at maximum transmit power, thereby resulting in a decrease in average energy consumption. In addition, the transmission success rate of ACT scheme is

Authorized licensed use limited to: University of Waterloo. Downloaded on March 04,2025 at 21:56:16 UTC from IEEE Xplore. Restrictions apply.

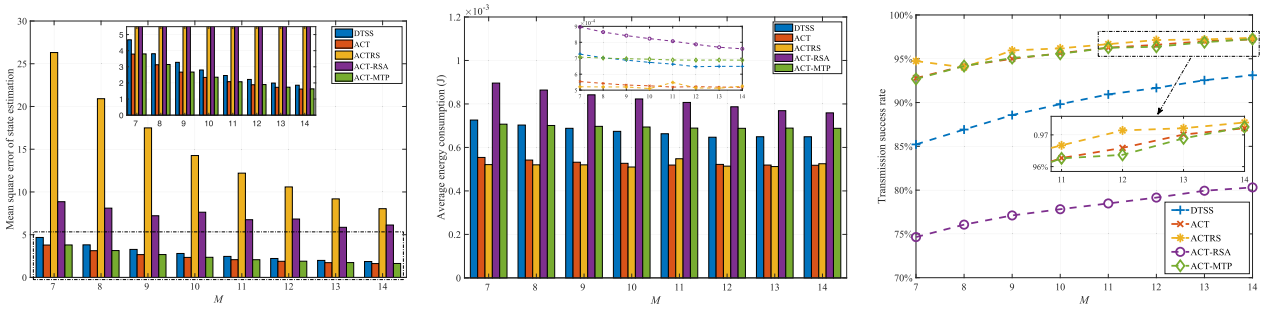

(a) (b) (c)

Fig. 9. Performance comparison with different number of subcarriers. (a) Mean square estimation error. (b) Average energy consumption. (c) Transmission success rate.

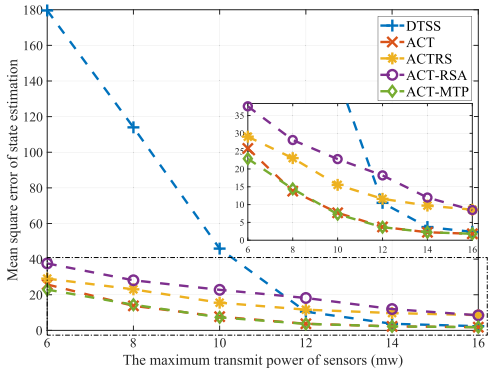

Fig. 10. Mean square estimation error comparison with different maximum transmit power of sensors.

consistently greater than that of DTSS scheme, consistently above 90%. The transmission success rate of ACT-RSA scheme is the lowest, basically below 80%. This indicates that in a spectrum-constrained environment, ACT scheme has a significant advantage in enhancing the reliability of data transmission.

The effect of sensor's maximum transmit power on the mean square estimation error is shown in Fig. 10. It can be seen that with the increase of maximum transmit power, the mean square estimation error with all schemes decreases sharply and then slowly decreases. Moreover, under the same maximum transmit power, the mean square error of ACT scheme is smallest. It verifies that ACT scheme has obvious advantages on improving the performance of state estimation.

V. Conclusion

In this paper, we investigated an AGV-assisted cooperative transmission in industrial IoT systems to improve the reliability of sensory data transmission and the accuracy of state estimation. We designed an ACT scheme to jointly optimize sensor scheduling and data transmission. In particular, the best transmission mode is chosen to deliver information according to the channel gain of line-of-sight transmission link between sensors and remote estimator. Moreover, only when the line-of-sight transmission link is heavily obstructed by AGV, the AGV-assisted cooperative transmission mode is activated. Then, an adaptive cooperative transmission algorithm was designed to maximize the amount of sensory data successfully received by the RE under the consideration of energy consumption. Simulation results show that ACT scheme can significantly improve estimation performance with low energy consumption. It is appropriate for applying the proposed adaptive cooperative transmission scheme into the area of smart manufacturing, since there are generally many moving obstacles and large metal equipments in the plant. Furthermore, the proposed scheme has advantage on the choosing adaptivity of transmission modes, which then could effectively enhance the transmission performance and estimation accuracy. For the future work, we will study sensor scheduling and data transmission in industrial IoT systems with heterogeneous sensor networks.

Appendix A
Proof of Theorem 1

The detailed expression of transmission energy consumption is given by

$$\begin{aligned} E_n^{\mathrm{T}}(k) &= \sum_{m\in\mathcal{M}} \theta_{n,m}(k) p_{n,m}^{\mathrm{S}}(k) t_n(k) \\ &= \sum_{m\in\mathcal{M}} \theta_{n,m}(k) p_{n,m}^{\mathrm{S}}(k) \Bigg((1-\delta_n(k)) \frac{q_n(k)}{R_n^{\mathrm{D}}(k)} \\ &\quad + \delta_n(k) \frac{q_n(k)}{R_n^{\mathrm{C}}(k)} \Bigg). \end{aligned} \tag{47}$$

It can be seen that the energy consumption expressions are different under different transmission modes. Therefore, we prove the monotonicity of the transmission energy consumption function under the two transmission modes respectively. To simplify the expression, the expression of single subcarrier transmission is adopted in the following.

case 1: $\delta_n(k) = 0$, the derivative of $E_n^{\mathrm{T}}(k)$ to $p_n^{\mathrm{S}}(k)$ can be expressed as

$$\frac{dE_n^{\mathrm{T}}(k)}{dp_{n,m}^{\mathrm{S}}(k)} = \frac{q_n(k)\left(\log_2\left(1+\Gamma_{n,m}^{\mathrm{D}}(k)\right) - \frac{\Gamma_{n,m}^{\mathrm{D}}(k)}{\left(1+\Gamma_{n,m}^{\mathrm{D}}(k)\right)\ln(2)}\right)}{B\log_2^2\left(1+\Gamma_{n,m}^{\mathrm{D}}(k)\right)}. \tag{48}$$

Authorized licensed use limited to: University of Waterloo. Downloaded on March 04,2025 at 21:56:16 UTC from IEEE Xplore. Restrictions apply.

Let $g_0(p^{\mathrm{S}}) = (1+\Gamma^{\mathrm{D}}_{n,m}(k)) - \frac{\Gamma^{\mathrm{D}}_{n,m}(k)}{(1+\Gamma^{\mathrm{D}}_{n,m}(k))\ln(2)}$. It can be seen that the monotonicity of $E^{\mathrm{T}}_n(k)$ depends on the size of the $g_0(p^{\mathrm{S}})$, if $g_0(p^{\mathrm{S}}) > 0$, $E^{\mathrm{T}}_n(k)$ is monotonically increasing, otherwise, $E^{\mathrm{T}}_n(k)$ is non-monotonically increasing. Let $g_0(p^{\mathrm{S}}) = 0$ to get $p^{\mathrm{S}}_{n,m}(k) = 0$, so the positive or negative value of the $g_0(p^{\mathrm{S}})$ can be determined by its monotonicity. Then, the derivative of $g_0(p^{\mathrm{S}})$ to $p^{\mathrm{S}}_{n,m}(k)$ is

$$\frac{dg_0(p^{\mathrm{S}})}{dp^{\mathrm{S}}_{n,m}(k)} = \frac{\Gamma^{\mathrm{D}}_{n,m}(k)}{\left(1+\Gamma^{\mathrm{D}}_{n,m}(k)\right)\ln(2)}, \tag{49}$$

where $\Gamma^{\mathrm{D}}_{n,m}(k) > 0$ when $p^{\mathrm{S}}_{n,m}(k) > 0$, so $g_0(p^{\mathrm{S}})$ is monotonically increasing when $p^{\mathrm{S}}_{n,m}(k) > 0$ (i.e., $g_0(p^{\mathrm{S}}) > 0$). Therefore, in the case of $\delta_n(k) = 0$, $E^{\mathrm{T}}_n(k)$ is monotonically increasing to $p^{\mathrm{S}}_{n,m}(k)$ when $p^{\mathrm{S}}_{n,m}(k) > 0$.

case 2: $\delta_n(k) = 1$, the derivative of $E^{\mathrm{T}}_n(k)$ to $p^{\mathrm{S}}_n(k)$ can be expressed as

$$\frac{\partial E^{\mathrm{T}}_n(k)}{\partial p^{\mathrm{S}}_{n,m}(k)} = \frac{q_n(k)\left(\log_2\left(1+\Gamma^{\mathrm{C}}_{n,m}(k)\right) - \frac{p^{\mathrm{S}}_{n,m}(k)\Gamma^{'\mathrm{,C}}_{n,m}(k)}{\left(1+\Gamma^{\mathrm{C}}_{n,m}(k)\right)\ln(2)}\right)}{B\log^2_2\left(1+\Gamma^{\mathrm{C}}_{n,m}(k)\right)}, \tag{50}$$

where $\Gamma^{'\mathrm{,C}}_{n,m}(k)$ is the partial derivative of $\Gamma^{\mathrm{C}}_{n,m}(k)$ to $p^{\mathrm{S}}_{n,m}(k)$. Let $g_1(p^{\mathrm{S}}, p^{\mathrm{A}}) = \log_2(1+\Gamma^{\mathrm{C}}_{n,m}(k)) - \frac{p^{\mathrm{S}}_{n,m}(k)\Gamma^{'\mathrm{,C}}_{n,m}(k)}{(1+\Gamma^{\mathrm{C}}_{n,m}(k))\ln(2)}$. Clearly, the monotonicity of $E^{\mathrm{T}}_n(k)$ depends on the size of the $g_1(p^{\mathrm{S}}, p^{\mathrm{A}})$. Similarly, let $g_1(p^{\mathrm{S}}, p^{\mathrm{A}}) = 0$ to get $p^{\mathrm{S}}_{n,m}(k) = 0$, thus the positive or negative value of the $g_1(p^{\mathrm{S}}, p^{\mathrm{A}})$ can be determined by its monotonicity. The partial derivative of $g_1(p^{\mathrm{S}}, p^{\mathrm{A}})$ to $p^{\mathrm{S}}_{n,m}(k)$ can be expressed as

$$\frac{\partial g_1(p^{\mathrm{S}}, p^{\mathrm{A}})}{\partial p^{\mathrm{S}}_{n,m}(k)} = \frac{p^{\mathrm{S}}_{n,m}\left(\left(\Gamma^{'\mathrm{,C}}_{n,m}(k)\right)^2 - \left(1+\Gamma^{\mathrm{C}}_{n,m}(k)\right)\Gamma^{''\mathrm{,C}}_{n,m}(k)\right)}{\left(1+\Gamma^{\mathrm{C}}_{n,m}(k)\right)^2\ln(2)}, \tag{51}$$

where $\Gamma^{''\mathrm{,C}}_{n,m}(k) = -\frac{2(\gamma^{\mathrm{SR}}_{n,m}(k)p^{\mathrm{A}}_{n,m}(k)\gamma^{\mathrm{AR}}_{n,m}(k))^2}{(p^{\mathrm{S}}_{n,m}(k)\gamma^{\mathrm{SA}}_{n,m}(k)+p^{\mathrm{A}}_{n,m}(k)\gamma^{\mathrm{AR}}_{n,m}(k))^3}$ is the second partial derivative of $g_1(p^{\mathrm{S}}, p^{\mathrm{A}})$ to $p^{\mathrm{S}}_{n,m}(k)$. $\Gamma^{\mathrm{C}}_{n,m}(k) > 0$, $\Gamma^{''\mathrm{,C}}_{n,m}(k) < 0$ when $p^{\mathrm{S}}_{n,m}(k) > 0$, so $g_1(p^{\mathrm{S}}, p^{\mathrm{A}})$ is monotonically increasing to $p^{\mathrm{S}}_{n,m}(k)$ when $p^{\mathrm{S}}_{n,m}(k) > 0$ (i.e., $g_1(p^{\mathrm{S}}, p^{\mathrm{A}}) > 0$). Therefore, in the case of $\delta_n(k) = 1$, $E^{\mathrm{T}}_n(k)$ is monotonically increasing to $p^{\mathrm{S}}_{n,m}(k)$ when $p^{\mathrm{S}}_{n,m}(k) > 0$.

REFERENCES

[1] S. F. Abedin, A. Mahmood, N. H. Tran, Z. Han, and M. Gidlund, "Elastic O-RAN slicing for industrial monitoring and control: A distributed matching game and deep reinforcement learning approach," *IEEE Trans. Veh. Technol.*, vol. 71, no. 10, pp. 10808–10822, Oct. 2022.

[2] Z. Yang, R. Wang, D. Wu, H. Wang, H. Song, and X. Ma, "Local trajectory privacy protection in 5G enabled industrial intelligent logistics," *IEEE Trans. Ind. Informat.*, vol. 18, no. 4, pp. 2868–2876, Apr. 2022.

[3] L. Lyu, C. Chen, N. Cheng, S. Zhu, X. Guan, and X. Shen, "NOMA-assisted on-demand transmissions for monitoring applications in industrial IoT networks," *IEEE Trans. Veh. Technol.*, vol. 69, no. 10, pp. 12264–12276, Oct. 2020.

[4] J. Hu, H. Zhang, B. Di, K. Bian, and L. Song, "Meta-IoT: Simultaneous sensing and transmission by meta-material sensor-based Internet of Things," *IEEE Trans. Wireless Commun.*, vol. 21, no. 8, pp. 6048–6063, Aug. 2022.

[5] Y. Zhang et al., "Resource scheduling for eMBB and URLLC multiplexing in NOMA-based VANETs: A dual time-scale approach," *IEEE Trans. Veh. Technol.*, early access, 28 Nov. 2023, doi: 10.1109/TVT.2023.3337250.

[6] L. Lyu, X. Guan, N. Cheng, and X. S. Shen, *Advanced Wireless Technologies for Industrial Network Systems*. Berlin, Germany: Springer, 2023.

[7] W. Wang et al., "Value matters: A novel value of information-based resource scheduling method for CAVs," *IEEE Trans. Veh. Technol.*, vol. 73, no. 6, pp. 8720–8735, Jun. 2024.

[8] H. Liu, P. Wang, J. Lin, H. Ding, H. Chen, and F. Xu, "Real-time longitudinal and lateral state estimation of preceding vehicle based on moving horizon estimation," *IEEE Trans. Veh. Technol.*, vol. 70, no. 9, pp. 8755–8768, Sep. 2021.

[9] L. Lyu, L. Zhao, and Y. Dai, "AoI-based priority-aware transmission scheduling for state estimation in industrial IoT systems," in *Proc. 5th Int. Conf. Commun., Signal Process., Appl.*, 2022, pp. 1–6.

[10] J. Chen, C. Yi, R. Wang, K. Zhu, and J. Cai, "Learning aided joint sensor activation and mobile charging vehicle scheduling for energy-efficient WRSN-based industrial IoT," *IEEE Trans. Veh. Technol.*, vol. 72, no. 4, pp. 5064–5078, Apr. 2023.

[11] Z. Qiao, L. Lyu, Y. Dai, N. Cheng, and X. Shen, "Energy-aware sensor scheduling and opportunistic transmission for state estimation in industrial IoT systems," in *Proc. IEEE/CIC Int. Conf. Commun. China*, 2023, pp. 1–6.

[12] A. Samanta, T. G. Nguyen, T. Ha, and S. Mumtaz, "Distributed resource distribution and offloading for resource-agnostic microservices in industrial IoT," *IEEE Trans. Veh. Technol.*, vol. 72, no. 1, pp. 1184–1195, Jan. 2023.

[13] M. Liu, L. Liu, H. Song, Y. Hu, Y. Yi, and F. Gong, "Signal estimation in underlay cognitive networks for industrial Internet of Things," *IEEE Trans. Ind. Informat.*, vol. 16, no. 8, pp. 5478–5488, Aug. 2020.

[14] J. Ding, S. Sun, J. Ma, and N. Li, "Fusion estimation for multi-sensor networked systems with packet loss compensation," *Inf. Fusion*, vol. 45, pp. 138–149, 2019.

[15] G. Yang, H. Rezaee, A. Serrani, and T. Parisini, "Sensor fault-tolerant state estimation by networks of distributed observers," *IEEE Trans. Autom. Control*, vol. 67, no. 10, pp. 5348–5360, Oct. 2022.

[16] W. Liu, D. E. Quevedo, Y. Li, K. H. Johansson, and B. Vucetic, "Remote state estimation with smart sensors over Markov fading channels," *IEEE Trans. Autom. Control*, vol. 67, no. 6, pp. 2743–2757, Jun. 2022.

[17] Y. Dai, L. Zhao, and L. Lyu, "MEC enabled cooperative sensing and resource allocation for industrial IoT systems," *China Commun.*, vol. 19, no. 7, pp. 214–225, 2022.

[18] Y. Feng, Y. Tan, G. Gu, and X. Chen, "Remote state estimation with enhanced robustness in the presence of data packet dropouts," *IEEE Trans. Autom. Control*, vol. 67, no. 12, pp. 6552–6566, Dec. 2022.

[19] L. Lyu, C. Chen, S. Zhu, X. Wen, and X. Guan, "Sensing aware opportunistic transmissions for situation monitoring in industrial network systems," in *Proc. IEEE Glob. Commun. Conf.*, 2019, pp. 1–6.

[20] L. Lyu, C. Chen, S. Zhu, N. Cheng, B. Yang, and X. Guan, "Control performance aware cooperative transmission in multiloop wireless control systems for industrial IoT applications," *IEEE Internet Things J.*, vol. 5, no. 5, pp. 3954–3966, Oct. 2018.

[21] Y. Li and L. Cai, "Cooperative device-to-device communication for uplink transmission in cellular system," *IEEE Trans. Wireless Commun.*, vol. 17, no. 6, pp. 3903–3917, Jun. 2018.

[22] Y. Dai, L. Lyu, and N. Cheng, "Impact of decoding order on user pairing in NOMA-CoMP joint transmission," *IEEE Trans. Veh. Technol.*, vol. 72, no. 7, pp. 9664–9669, Jul. 2023.

[23] Z. Mao, F. Hu, D. Sun, S. Ma, and X. Liu, "Fairness-aware intra-group cooperative transmission in wireless powered communication networks," *IEEE Trans. Veh. Technol.*, vol. 69, no. 6, pp. 6463–6472, Jun. 2020.

[24] P. Xu, J. Quan, G. Chen, Z. Yang, Y. Li, and I. Krikidis, "A novel link selection in coordinated direct and buffer-aided relay transmission," *IEEE Trans. Wireless Commun.*, vol. 22, no. 5, pp. 3296–3309, May 2023.

[25] N. T. Tuan, D. S. Kim, and J. M. Lee, "On the performance of cooperative transmission schemes in industrial wireless sensor networks," *IEEE Trans. Ind. Informat.*, vol. 14, no. 9, pp. 4007–4018, Sep. 2018.

[26] T. Kim and D. Qiao, "Energy-efficient data collection for IoT networks via cooperative multi-hop UAV networks," *IEEE Trans. Veh. Technol.*, vol. 69, no. 11, pp. 13796–13811, Nov. 2020.

[27] S. H. Chae and K. Lee, "Cooperative relaying for multi-user MIMO wireless backhaul networks," *IEEE Trans. Veh. Technol.*, vol. 70, no. 3, pp. 2794–2806, Mar. 2021.

[28] S. Girs, A. Willig, E. Uhlemann, and M. Björkman, "Scheduling for source relaying with packet aggregation in industrial wireless networks," *IEEE Trans. Ind. Informat.*, vol. 12, no. 5, pp. 1855–1864, Oct. 2016.

Authorized licensed use limited to: University of Waterloo. Downloaded on March 04,2025 at 21:56:16 UTC from IEEE Xplore. Restrictions apply.

[29] H. Hu, X. Jia, K. Liu, and B. Sun, "Self-adaptive traffic control model with behavior trees and reinforcement learning for AGV in industry 4.0," *IEEE Trans. Ind. Informat.*, vol. 17, no. 12, pp. 7968–7979, Dec. 2021.
[30] J. Lin, P. Yang, N. Zhang, F. Lyu, X. Chen, and L. Yu, "Low-latency edge video analytics for on-road perception of autonomous ground vehicles," *IEEE Trans. Ind. Informat.*, vol. 19, no. 2, pp. 1512–1523, Feb. 2023.
[31] L. Lyu, C. Chen, S. Zhu, and X. Guan, "5G enabled codesign of energy-efficient transmission and estimation for industrial IoT systems," *IEEE Trans. Ind. Informat.*, vol. 14, no. 6, pp. 2690–2704, Jun. 2018.
[32] J. Liu, M. Sheng, L. Liu, and J. Li, "Performance of small cell networks under multislope bounded pathloss model: From sparse to ultradense deployment," *IEEE Trans. Veh. Technol.*, vol. 67, no. 11, pp. 11022–11034, Nov. 2018.
[33] M. Hasna and M.-S. Alouini, "End-to-end performance of transmission systems with relays over Rayleigh-fading channels," *IEEE Trans. Wireless Commun.*, vol. 2, no. 6, pp. 1126–1131, Nov. 2003.
[34] J. Tang and X. Zhang, "Cross-layer resource allocation over wireless relay networks for quality of service provisioning," *IEEE J. Sel. Areas Commun.*, vol. 25, no. 4, pp. 645–656, May 2007.
[35] P. Li, S. Guo, and W. Zhuang, "Optimal transmission scheduling of cooperative communications with a full-duplex relay," *IEEE Trans. Parallel Distrib. Syst.*, vol. 25, no. 9, pp. 2353–2363, Sep. 2014.
[36] A. S. Leong, D. E. Quevedo, D. Dolz, and S. Dey, "Transmission scheduling for remote state estimation over packet dropping links in the presence of an eavesdropper," *IEEE Trans. Autom. Control*, vol. 64, no. 9, pp. 3732–3739, Sep. 2019.
[37] J. Zhou, G. Gu, and X. Chen, "Distributed Kalman filtering over wireless sensor networks in the presence of data packet drops," *IEEE Trans. Autom. Control*, vol. 64, no. 4, pp. 1603–1610, Apr. 2019.
[38] Y. Yilmaz, M. N. Kurt, and X. Wang, "Distributed dynamic state estimation and LQG control in resource-constrained networks," *IEEE Trans. Signal Inf. Process. Netw.*, vol. 4, no. 3, pp. 599–612, Sep. 2018.
[39] S.-L. Sun and Z.-L. Deng, "Multi-sensor optimal information fusion Kalman filter," *Automatica*, vol. 40, no. 6, pp. 1017–1023, 2004.
[40] S. Zoppi, T. Soleymani, M. Klügel, M. Vilgelm, S. Hirche, and W. Kellerer, "Transmission power control for remote state estimation in industrial wireless sensor networks," 2019, *arXiv:1907.07018*.
[41] Q. Voortman, D. Efimov, A. Pogromsky, J.-P. Richard, and H. Nijmeijer, "Remote state estimation of steered systems with limited communications: An event-triggered approach," *IEEE Trans. Autom. Control*, vol. 69, no. 7, pp. 4199–4214, Jul. 2024.
[42] D. Feng, L. Lu, Y. Yuan-Wu, G. Y. Li, G. Feng, and S. Li, "Device-to-device communications underlaying cellular networks," *IEEE Trans. Commun.*, vol. 61, no. 8, pp. 3541–3551, Aug. 2013.
[43] S. Mu, Z. Zhong, D. Zhao, and M. Ni, "Joint job partitioning and collaborative computation offloading for Internet of Things," *IEEE Internet Things J.*, vol. 6, no. 1, pp. 1046–1059, Feb. 2019.
[44] E. Bedeer, A. Alorainy, M. J. Hossain, O. Amin, and M.-S. Alouini, "Fairness-aware energy-efficient resource allocation for AF co-operative OFDMA networks," *IEEE J. Sel. Areas Commun.*, vol. 33, no. 12, pp. 2478–2493, Dec. 2015.

Ling Lyu (Member, IEEE) received the B.S. degree in telecommunication engineering from Jinlin University, Changchun, China, in 2013, and the Ph.D. degree in control theory and control engineering from Shanghai Jiao Tong University, Shanghai, China, in 2019. In 2019, she joined Dalian Maritime University, Dalian, China, where she is currently an Associate Professor with the School of Information Science and Technology. She was a Visiting Student with University of Waterloo, Waterloo, ON, Canada from 2017 to 2018. Her current research interests include wireless sensor and actuator network and application in industrial automation, the joint design of communication and control in industrial cyber-physical systems, estimation and control over lossy wireless networks, machine type communication enabled reliable transmission in the fifth generation network, resource allocation, energy efficiency.

Zexin Qiao received the B.Eng. degree in communication engineering from the Taiyuan Institute of Technology, Taiyuan, China, in 2021. He is currently working toward the M.Eng. degree with Dalian Maritime University, Dalian, China. His research interests include resource allocation and state estimation.

Yanpeng Dai (Member, IEEE) received the B.Eng. degree from Shandong Normal University, Jinan, China, in 2014, and the Ph.D. degree from Xidian University, Xi'an, China, in 2020. He is currently an Associate Professor with the College of Information Science and Technology, Dalian Maritime University, Dalian, China. His research interests include resource management and interference coordination of heterogeneous wireless networks.

Nan Cheng (Senior Member, IEEE) received the B.E. and M.S. degrees from the Department of Electronics and Information Engineering, Tongji University, Shanghai, China, in 2009 and 2012, respectively, and the Ph.D. degree from the Department of Electrical and Computer Engineering, University of Waterloo, Waterloo, ON, Canada, in 2016. From 2017 to 2019, he was a Postdoctoral Fellow with the Department of Electrical and Computer Engineering, University of Toronto, Toronto, ON, Canada. He is currently a Professor with the State Key Laboratory of ISN and with School of Telecommunications Engineering, Xidian University, Xi'an, China. He has authored or coauthored more than 90 journal papers in IEEE Transactions and other top journals. His research interests include B5G/6 G, AI-driven future networks, and space-air-ground integrated network. He is an Associate Editors for IEEE TRANSACTIONS ON VEHICULAR TECHNOLOGY, IEEE OPEN JOURNAL OF THE COMMUNICATIONS SOCIETY, and *Peer-to-Peer Networking and Applications*. He is/was the Guest Editors of several journals.

Cailian Chen (Member, IEEE) received the B.Eng. and M.Eng. degrees in automatic control from Yanshan University, Qinhuangdao, China, in 2000 and 2002, respectively, and the Ph.D. degree in control and systems from the City University of Hong Kong, Hong Kong, in 2006. She has been with the Department of Automation, Shanghai Jiao Tong University, Shanghai, China, since 2008. She is currently a Distinguished Professor. She has authored three research monographs and more than 100 refereed international journal articles. She is the inventor of more than 30 patents. Her research interests include industrial wireless networks and computational intelligence and the Internet of Vehicles. Dr. Chen received the prestigious IEEE Transactions on Fuzzy Systems Outstanding Paper Award in 2008, IEEE TCCPS Industrial Technical Excellence Award in 2022, and five conference best paper awards. She was awarded N2Women Star in Computer Networking and Communications in 2022. She was the recipient of the Second Prize of National Natural Science Award from the State Council of China in 2018, First Prize of Natural Science Award from The Ministry of Education of China in 2006 and 2016, respectively, and First Prize of Technological Invention of Shanghai Municipal, China, in 2017. She was honored "National Outstanding Young Researcher" by NSF of China in 2020, "Changjiang Young Scholar" in 2015, and China Young Women Scientists Award in 2023. She has been actively involved in various professional services. She is a Distinguished Lecturer of IEEE VTS. She is a Deputy Editor for *National Science Open* and an Associate Editor for IEEE TRANSACTIONS ON VEHICULAR TECHNOLOGY and *IET Cyber-Physical Systems: Theory & Applications*.

Authorized licensed use limited to: University of Waterloo. Downloaded on March 04,2025 at 21:56:16 UTC from IEEE Xplore. Restrictions apply.

Xinping Guan (Fellow, IEEE) is currently a Chair Professor with Shanghai Jiao Tong University, Shanghai, China, where he is also the Dean of the School of Electronic, Information and Electrical Engineering and the Director of the Key Laboratory of Systems Control and Information Processing, Ministry of Education of China. Before that, he was the Executive Director of Office of Research Management with Shanghai Jiao Tong University and a Full Professor and the Dean of Electrical Engineering with Yanshan University, Qinhuangdao, China. He has authored and/or co-authored five research monographs, more than 200 papers in peer-reviewed journals, and numerous conference papers. His current research interests include industrial network systems, smart manufacturing, and underwater networks. As a Principal investigator, he has finished/been working on more than 20 national key projects. He is the Leader of the prestigious Innovative Research Team of the National Natural Science Foundation of China (NSFC). Dr. Guan is an Executive Committee Member of Chinese Automation Association Council and Chinese Artificial Intelligence Association Council. He was the recipient of the First Prize of Natural Science Award from the Ministry of Education of China in 2006 and 2016 and the Second Prize of the National Natural Science Award of China in 2008 and 2018. He was a recipient of IEEE Transactions on Fuzzy Systems Outstanding Paper Award in 2008 and IEEE TCCPS Industrial Technical Excellence Award in 2022. He was honored National Outstanding Youth by NSF of China, Changjiang Scholar by the Ministry of Education of China and State-Level Scholar of New Century Bai Qianwan Talent Program of China.

Xuemin (Sherman) Shen (Fellow, IEEE) received the Ph.D. degree in electrical engineering from Rutgers University, New Brunswick, NJ, USA, in 1990. He is currently a University Professor with the Department of Electrical and Computer Engineering, University of Waterloo, Waterloo, ON, Canada. His research interests include network resource management, wireless network security, Internet of Things, 5G and beyond, and vehicular networks. Dr. Shen is a registered Professional Engineer of Ontario, Canada, an Engineering Institute of Canada Fellow, a Canadian Academy of Engineering Fellow, a Royal Society of Canada Fellow, a Chinese Academy of Engineering Foreign Member, and an International Fellow of the Engineering Academy of Japan. Dr. Shen was the recipient of the West Lake Friendship Award from Zhejiang Province in 2023, President's Excellence in Research from the University of Waterloo in 2022, the Canadian Award for Telecommunications Research from the Canadian Society of Information Theory (CSIT) in 2021, the R.A. Fessenden Award in 2019 from IEEE, Canada, Award of Merit from the Federation of Chinese Canadian Professionals (Ontario) in 2019, James Evans Avant Garde Award in 2018 from the IEEE Vehicular Technology Society, Joseph LoCicero Award in 2015 and Education Award in 2017 from the IEEE Communications Society (ComSoc), and Technical Recognition Award from Wireless Communications Technical Committee (2019) and AHSN Technical Committee in 2013. He was also the recipient of the Excellent Graduate Supervision Award in 2006 from the University of Waterloo and the Premier's Research Excellence Award (PREA) in 2003 from the Province of Ontario, Canada. He is/was the General Chair for the 6 G Global Conference'23, and ACM Mobihoc'15, Technical Program Committee Chair/Co-Chair for IEEE Globecom'24, 16 and 07, IEEE Infocom'14, IEEE VTC'10 Fall, and the Chair for the IEEE ComSoc Technical Committee on Wireless Communications. Dr. Shen is the Past President of the IEEE ComSoc, the Vice President for Technical & Educational Activities, Vice President for Publications, Member-at-Large on the Board of Governors, Chair of the Distinguished Lecturer Selection Committee, and Member of IEEE Fellow Selection Committee of the ComSoc. Dr. Shen was the Editor-in-Chief of the IEEE INTERNET OF THINGS JOURNAL, IEEE NETWORK, and PPNA.

Authorized licensed use limited to: University of Waterloo. Downloaded on March 04,2025 at 21:56:16 UTC from IEEE Xplore. Restrictions apply.